JGR Atmospheres

RESEARCH ARTICLE
10.1029/2022JD036681

Surface Potential Gradients and NEXRAD Radar Reflectivities Before the Onset of Lightning at the KSC-ER

S. C. Handel[1], K. L. Cummins[2], and E. P. Krider[2]

[1]NOAA Climate Prediction Center, College Park, MD, USA, [2]Department of Hydrology and Atmospheric Sciences, University of Arizona, Tucson, AZ, USA

Key Points:

- Elevated surface potential gradients precede lightning in both the early and late stages of thunderstorms
- Electrification in cumulus clouds can begin before the 0 dBZ radar cloud top reaches the −20°C level and within 4–5 min after it reaches the −10°C level
- Initial electrification often indicated the presence of a localized lower positive charge region that was sometimes enhanced by early intracloud discharges

Supporting Information:

Supporting Information may be found in the online version of this article.

Correspondence to:

K. L. Cummins,
kcummins@arizona.edu

Citation:

Handel, S. C., Cummins, K. L., & Krider, E. P. (2022). Surface potential gradients and NEXRAD radar reflectivities before the onset of lightning at the KSC-ER. *Journal of Geophysical Research: Atmospheres*, *127*, e2022JD036681. https://doi.org/10.1029/2022JD036681

Received 27 FEB 2022
Accepted 31 AUG 2022

Author Contributions:

Conceptualization: S. C. Handel, K. L. Cummins, E. P. Krider
Data curation: K. L. Cummins
Formal analysis: S. C. Handel, K. L. Cummins
Funding acquisition: E. P. Krider
Investigation: S. C. Handel, K. L. Cummins, E. P. Krider
Methodology: E. P. Krider
Visualization: S. C. Handel
Writing – original draft: S. C. Handel, K. L. Cummins, E. P. Krider

Abstract Measurements provided by Next Generation Weather Radar and operational thunderstorm monitoring instruments at the Kennedy Space Center and the Air Force Eastern Range have been examined to determine the initial electrical development of 13 isolated, air mass thunderstorms. The same instruments were used to examine the surface potential gradient prior to and following 13 long, horizontal discharges that propagated into the area. The motivation and primary objective for this work was to evaluate the safety of the existing lightning-related launch constraints associated with surface potential gradient and precipitation radar measurements. The onset of cloud electrification as seen by a large-area surface electric field mill network was detected 3.7–14.6 min before the first lightning discharge, with lead-times that depended on proximity to the storm. In 11 of 13 cases, the first detectable field change was a positive excursion in potential gradient close to the storm, likely indicating initial development of lower positive charge. Lead-times for the radar-derived cloud tops (0 dBZ) reaching −20°C were longer than those for early electrification in all but two cases. Surface potential gradients above +500 V/m or below −100 V/m "warning thresholds" were exceeded before the first lightning flash in all cases. Radar reflectivities >35 dBZ above the −10°C level provided 3–14 min of lead time for lightning. Potential gradients just prior to and near long horizontal discharges exceeded 3 kV/m at most sites and were typically positive. Measurements at a single field mill site would not have provided adequate warning.

1. Introduction

The NASA Kennedy Space Center and Air Force Eastern Range (KSC-ER) are located on the East coast of central Florida, one of the regions of highest thunderstorm activity in the United States. Annually, dozens of lightning-sensitive spacecraft and payloads are launched from this site, which makes effective warning of potential natural or triggered lightning threats imperative. Previous incidents of space vehicles triggering lightning, such as Apollo 12 (Arabian, 1970; Godfrey et al., 1970) and Atlas/Centaur 67 (Christian et al., 1989), underscore the seriousness of this threat. These incidents have led to today's "Natural and Triggered Lightning Launch Commit Criteria" (LLCC—see NASA-STD-4010, 2017) that have been prepared by the NASA/USAF Lightning Advisory Panel (LAP). The rationale behind these requirements and the structure of the LLCC is provided in Willett et al. (2016). Its companion "History Document" (Merceret et al. (2010)) reviews the origins and evolution of the LLCC, the history and function of the LAP, and implementation and verification of the rules by the weather-support organizations and infrastructure at the KSC-ER.

Three hazards that are particularly difficult to forecast and detect are the initial electrification of isolated thunderstorms over the KSC-ER area, the first flash in a storm, and the propagation of long, horizontal flashes into the area from deep convection outside but near this domain. Because of these factors, the KSC-ER currently maintains a comprehensive, large-area network of ground-based electric field mills that can detect electrified clouds prior to the occurrence of lightning and thereby warn of potential lightning hazards. Precipitation radar has also proved to be very useful in anticipating cloud electrification and lightning. Early work in atmospheric electricity has clearly shown there is a good correlation between precipitation radar reflectivity and elevated surface potential gradients (Reynolds & Brook, 1956; Workman & Reynolds, 1949), with both preceding the occurrence of lightning to varying degrees. Radar reflectivity is also spatially and temporally correlated with the occurrence of long, horizontal discharges, because such discharges have been shown to propagate preferentially (but not exclusively) in/near regions that have reflectivity above 10 dBZ (Mecikalski & Carey, 2018) or above/below a radar bright band (Wang et al., 2019).

Writing – review & editing: S. C. Handel, K. L. Cummins, E. P. Krider

Here, we analyze data derived from the KSC-ER field mill network, a suite of lightning detection systems, and Next Generation Weather Radar (NEXRAD) sites at Melbourne and Tampa (48 and 198 km from the center of the KSC-ER, respectively) to determine how the electric fields and lightning developed in space and time near the beginning of isolated storms. We use these same instruments to study the spatial distributions of the surface potential gradient and radar reflectivity before long, horizontal flashes propagated into the KSC-ER from nearby storms.

The motivation and primary objective for this work is to evaluate the safety of the existing LLCC constraints associated with surface potential gradient and precipitation radar measurements. The findings associated with initial electrification exposed quite interesting spatial and temporal patterns of surface potential gradient that caused us to explore these cases and the related literature to a greater degree than the cases of long horizontal discharges. We believe that these case studies, only 13 for each condition, demonstrate the need for larger and more-detailed studies for both conditions, using more-recent observations at KSC that include better lightning mapping, faster radar volume scans, and dual-polarization radar information. Such larger studies might also be able to address false-alarm rates, which is not practical in this small case study.

Section 2 provides some background on the physical processes and historical observations related to thunderstorm electrification and decay, and their relationship to lightning. The instrumentation and measurements used in this study are described in Section 3, and an overview of the cases in this study is given in Section 4. Our findings are described in Sections 5–8.

2. Background

The polarity of the atmospheric electric field is central to this work and is a source of confusion when one looks at the existing literature. More specifically, some studies have used the term "electric field" when potential gradient measurements (negative of the electric field) were employed. For potential gradient (hereafter PG), positive values in the vertical direction indicate a dominant positive charge overhead, weighted by distance. The fair-weather vertical PG measured at the earth's surface is positive, varying in a diurnal pattern between about 100 and 200 V/m at flat, undisturbed locations (Harrison, 2013; Lucas et al., 2017). During the developing and early mature stages of thunderstorms, the PG at the surface is typically negative (Livingston & Krider, 1978) and is frequently referred to as the "foul-weather polarity." In this section, we employ the terms "electric field" and "PG" in accordance with our best estimate of the polarity convention used by the cited authors, when polarity is relevant to the interpretation of the findings.

2.1. Thunderstorm Charge Structure and Initial Electrification

It has long been known that air mass thunderstorms produce two or more vertically separated regions of charge that have opposite polarity (Wilson, 1920). In 1929, Wilson (1929) deduced that the upper charge center was typically positive and the lower charge center was negative. Later, the typical mature thunderstorm was found to be described better by including a third, lower positive charge center (LPCC), as discussed in detail by Williams (1989), although this too has been shown to be somewhat of an over-simplification in some cases (Stolzenburg & Marshall, 2008; Stolzenburg et al., 1998, 2002).

One of the first investigators to suggest the presence of a localized region of positive charge in the lower portion of a thundercloud was Simpson (1927), who also hypothesized that this localized positive charge center was created by the breakup of water drops in regions of strong updrafts in the lower part of the cloud, with the larger water drops retaining positive charge and negative charge was given to the air (Simpson, 1909). This hypothesis was refined using potential gradient measurements aloft which provided clear evidence of a tri-polar structure of a large percentage of thunderstorms. Detailed reviews of the history and the scientific disagreement between Wilson and Simpson of this topic, resulting from different perspectives and measurement methods, is provided by Williams (1989, 2009).

Charge separation mechanisms in thunderclouds are discussed in detail by Krehbiel (1986), Saunders (2008), and Stolzenburg and Marshall (2008). Broad treatments of thunderstorm development, cloud electrification, and their relationship to weather and climate can be found in Krehbiel (1986) and Black and Hallett (1998). These reports and the studies they cite show that charge separation is dependent on several factors including temperature, liquid

water content of the cloud, size of the hydrometeors, and the velocity associated with the graupel-ice crystal collisions. This noninductive ice-graupel charging mechanism is thought to be primarily responsible for the upper-level charge separation necessary for "typical" IC discharges, and can also be used to explain the presence of descending positively charged graupel at temperatures warmer than about −15°C, likely leading to the development of lower positive charge (Phillips et al., 2020; Williams, 1989).

There are other mechanisms that could contribute to creating or expanding lower positive charge (see Williams (1989)), but the most reasonable alternative explanation during initial electrification, at least in areas with significant low-level moisture leading to low cloud bases (such as Florida), is the precipitation drop break-up mechanism mentioned above. This mechanism was pursued in detail by Simpson and co-workers (Simpson, 1909; Simpson & Robinson, 1941; Simpson & Scrase, 1937), and does not require an existing electric field, recent lightning, or large precipitation particles reaching above the freezing level. It could logically result in positive charge descending toward ground during initial electrification in developing cumulus clouds, producing fair-weather polarity surface potential gradients. Evidence of large raindrops during initial cumulus development, both above and below the melting level and descending toward ground prior to the occurrence of lightning, is provided in Mattos et al. (2017), and the references cited therein. As discussed by Williams (2009), this mechanism is not a candidate for producing the mid- and upper-level charge regions, but it cannot be ruled out as a contributor to the early development of a lower positive charge region.

In addition to the main charge separation processes discussed above, Jacobson and Krider (1976) and Holden et al. (1983) found evidence that lightning discharges themselves may play an important role in creating, reducing, or expanding the LPCC. In both studies, it was observed that positive offsets in the potential gradient (enhanced fair-weather polarity PG) at ground can be produced by nearby lightning discharges. Later work by Murphy (1996) found that out of 57 positive offsets in the surface PG that were analyzed in thunderstorms at KSC-ER, the majority (65%) were initiated at the time of lightning discharges. Murphy (1996) also found that 59% of these flashes were IC discharges between the upper positive and main negative charge centers. This concept of "charge deposition" by lightning is supported by in situ measurements in two storms using instrumented aircraft (Mo et al., 2002), and by detailed analysis of balloon soundings of in-cloud electric field, surface electric field, and 3-dimensional lightning mapping (Coleman et al., 2003). However, there is still no universal agreement about the contribution of lightning to the creation or evolution of the LPCC (Williams, 1989). Nonetheless, these early discharges do result in dramatic changes in the nearby quasi-static PG measured at the surface, including rapid changes in polarity that can last for several minutes.

2.2. Detection of Initial Electrification Using Surface Electric Field Measurements

Studies of the surface PG associated with the initial electrification of thunderstorms began in the mid-twentieth century (Reynolds & Brook, 1956; Workman & Reynolds, 1949). In these studies, the onset of electrification was defined as the time when a storm-related field disturbance was first detected at the ground. This same definition will be used here. To date, the latency between first detection of a disturbed field at the earth's surface and the charge separation aloft is not well known. A study by Vonnegut et al. (1959) evaluated early electrification using PG measurements on a tethered balloon just below the freezing level. The measured PG indicated the presence of nearby positive charge that preceded a deviation from fair-weather values at the ground by more than 10 min. Conversely, simultaneous observations of aircraft-based in-cloud and surface electric fields during initial development were reported by Dye et al. (1989), who found no significant delays in the surface-measured onset of electrification. We are not aware of any additional measurements that refute the observations by Vonnegut et al. (1959), and it is not unreasonable to think that there can be vertical charge distributions in small developing thunderstorms that produce large electric fields aloft, but exhibit very small fields at the ground. One such case in Florida has been described in detail by Karunarathna et al. (2017), where the field at the ground did not exceed a foul-weather magnitude of 200 V/m prior to the first lightning in the parent cumulus cloud. The two closest EFM sensors to the convective core recorded smaller initial field values than that site at a distance of about 7 km that reached 200 V/m. In this case, the 40 dBZ radar echo in the developing cell reached 7.1 km (about −15°C in most summer thunderstorms at the KSC-ER) several minutes before any indication of disturbed field at the ground, and about 9 min before the first lightning flash.

The polarity of the initial electrification as seen at ground is poorly quantified and clearly depends on the vertical charge structure and horizontal distance to the storm (Simpson & Robinson, 1941). Workman and Reynolds

(Workman & Reynolds, 1949) and Reynolds and Brook (Reynolds & Brook, 1956) found that the initial electrification (PG) at ground was typically negative in New Mexico, although later work (Moore & Vonnegut, 1977; Vonnegut et al., 1959) provided some evidence of an initial positive offset in PG at the surface and close to the storm. Later, Murphy (1996) and others found that the onset of surface PG disturbances directly below a developing storm is frequently positive, likely due to the formation of a LPCC. This initial positive PG detected at the ground and close to the storm likely disappears when larger and more wide-spread negative charge forms at higher altitudes (Murphy, 1996). Stolzenburg et al. (2015) show cases of isolated New Mexico storms that exhibited both initial polarities. Conceptually, for a simple, idealized stacked tripolar point-charge structure (a lower positive charge, a mid-level negative charge, and an upper positive charge), the surface PG can be small or positive directly below these charges, reach a negative maximum within a horizontal displacement along the ground of a few km, and then reverse again or become small beyond 5–10 km (Simpson and Robinson (1941), Rakov and Uman (2003), Section 3.2).

2.3. Characterization of the First Lightning Discharge

There is a clear preference for an IC discharge to occur first within a developing storm. Previous studies such as Workman and Reynolds (1949), Lhermitte and Krehbiel (1979), and Williams et al. (1989) among others found that IC discharges typically precede the initial CG flash. Williams et al. (1989) suggested that this was true in a variety of geographical locations and storm types. In fact, MacGorman and Rust (1998) note that by the late 1990's, only one published paper (Krehbiel, 1986) even discussed a case where the initial lightning discharge was a CG flash. With the development and deployment of modern VHF lightning mapping systems (Rison et al., 1999; Thomas et al., 2004) and wide-area CG lightning observations (Cummins & Murphy, 2009), it became practical to obtain long-term observations of both types of lightning in a variety of locations. Using these systems, MacGorman et al. (2011) found that the percentage of storms in which CG lightning was reported in the first minute varied by region, from 0% in the northern U.S. high plains, and up to 20% in Oklahoma and North Texas.

2.4. Lead-Times Before First Lightning Discharge

Dye et al. (1989) found that the initial electrification aloft (>1 kV/m) lagged the radar reflectivity reaching 40 dBZ above 6 km (about −10°C), typically by 1–14 min. The lead-time for this radar metric ranged from 4 to 33 min (when lightning occurred), with a median value between 11 and 16 min (computed using their Table 2). This study found no evidence of charge separation, using both aircraft and surface electric field measurements, prior to the radar reflectivity becoming greater than 36 dBZ above the −10°C level and with visible cloud tops well above −20°C. This study had exceptional radar coverage, using two well-calibrated radars operating at a 5-cm wavelength and that were located within 40 km of the storms, and with 3-min volume scan intervals. These data were also supplemented by other nearby radars to determine cloud top height. The time-history of maximum reflectivity and cloud top height were constructed for these cases, interpolating between the volume scans. Findings from a recent but smaller study in New Mexico by Stolzenburg et al. (2015) were consistent with those of Dye et al. (1989, 2007).

Numerous other studies support the finding by Dye et al. (1989) that radar provides long lead-times prior to lightning occurrence. Prior work summarized in Mosier et al. (2011) reported lead-times for lightning between 4 and 33 min; their detailed study found average lead-times between 7.5 and 15 min for well-qualified cases depending on reflectivity and temperature levels used. A later study by Seroka et al. (2012) considered both IC and CG flashes in Florida, and found similar average lead times for CG lightning as Mosier et al. when using a threshold reflectivity of 20 dBZ at −10°C level. These findings will be discussed further below, in the light of the results presented here.

2.5. Long, Horizontal Flashes

Long, horizontal lightning discharges have been known to propagate over distances of several tens of kilometers or more, and frequently produce large changes in the surface PG. Early studies using high time-resolution radar observations have identified horizontal flashes over 100 km long (Atlas, 1958; Ligda, 1956), with recent findings of many flashes with horizontal extents greater than 500 km (Peterson, 2021). Evidence of a horizontal

structure of lightning was identified in the early 1940's (Workman et al., 1942) and supported by later works by Pierce (1955), Ogawa and Brook (1969), and Teer and Few (1974). Shao and Krehbiel (1996) found that lightning discharges tend to propagate horizontally in layers corresponding to positive and negative charge regions, and this has been further supported by later work (Coleman et al., 2003, 2008; Medina et al., 2021; Van Der Velde et al., 2010). Krehbiel (1986), Maier, Lennon, Krehbiel, et al. (1995), and Maier, Lennon, Britt, and Schaefer (1995) among others have indicated that flashes become increasingly horizontal and extensive as a storm evolves. In addition, numerous studies have suggested that lightning discharges can propagate through two or more cells and penetrate into anvils or debris clouds, accentuating their horizontal extent (MacGorman et al., 1983; Mazur & Rust, 1983; Proctor, 1983; Scott et al., 1995).

Horizontally extensive flashes are common in the trailing stratiform regions of large multicellular convective systems and in anvils associated with large storms and supercells. Stratiform flashes often are associated with nearby radar bright bands and typically occur where maximum nearby reflectivity values are greater than 24 dBZ (Wang et al., 2020) in the cloud. Anvil flashes have been shown to be initiated near local reflectivity maxima, within screening layers at cloud boundaries, and at intersections of anvils from adjoining storms (Kuhlman et al., 2009; Weiss et al., 2012).

In the later stages of thunderstorms, high surface PGs can exist below horizontal extension of anvils and stratiform regions. In the simplest form, the surface PG below an anvil will be positive due to a large, advected positive charge layer between lesser negative screening layers. However, more complex charge structures can exist and can vary throughout the anvil and stratiform regions (Dye et al., 2007; Shepherd et al., 1996; Stolzenburg & Marshall, 2008; Williams, 1998).

Finally, surface PG polarity can reverse following a horizontally extensive flash overhead. For example, Moore and Vonnegut (Moore & Vonnegut, 1977) concluded that large positive PGs at the ground can arise when lower negative charge is displaced or removed, exposing positive charge at higher altitude in the cloud.

We are unaware of studies giving a detailed analysis of the surface PG immediately before and after the propagation of long, horizontal discharges over a field mill network. However, large electric fields have been shown to persist well beyond the time of last flash, seen using sequential balloon electric field soundings and surface electric field measurements (Stolzenburg et al., 2010). Several studies have demonstrated that surface PGs typically remain high for a period known as the End of Storm Oscillation (EOSO) even after the final lightning flash (Krehbiel, 1986; Livingston & Krider, 1978; Marshall et al., 2009; Moore & Vonnegut, 1977; Pawar & Kamra, 2007). Forbes and Hoffert (1999) found that the ground-level PGs typically remain high (>1 kV/m) for tens of minutes after the last CG flash using the field mill network employed in this study, but they did not address lightning aloft. Livingston and Krider found that time- and area-average surface PG was 2–4 times larger during the EOSO than during periods of intense lightning. It is reasonable to expect that surface PGs would be high prior to the initiation of long, horizontal discharges, with significantly different values after the flash.

3. Instrumentation

During the observation period for this work, there were three lightning detection systems operating at the KSC-ER that were relied on heavily in this study. These were a large-area network of surface electric field mills known as the Launch Pad Lightning Warning System (LPLWS) (Jacobson & Krider, 1976), a Cloud-To-Ground Lightning Surveillance System (CGLSS) (Wilson et al., 2009), and a Lightning Detection and Ranging (LDAR) lightning mapping system (Boccippio et al., 2001a, 2001b). In addition, the NEXRAD precipitation radar (Klazura & Imy, 1993) located at Tampa and Melbourne Florida provided cloud reflectivity for all but two of the cases in this study. The presence of these operational systems, all covering the same area, provided a unique opportunity for detailed analysis of the time-evolution of surface electric fields, radar reflectivity, and lightning.

3.1. Launch Pad Lightning Warning System

The field mill network at the KSC-ER contained 31 sensors at the time of this study, and covered an area of roughly 600 square kilometers, as shown in Figure 1. The separation distance between sensors was generally 2–4 km, with a few as large as 5 km. Each electric field mill (EFM) measured the static and quasi-static vertical component of the PG (negative electric field) at ground level. The data were digitized at a rate of 50 Hz

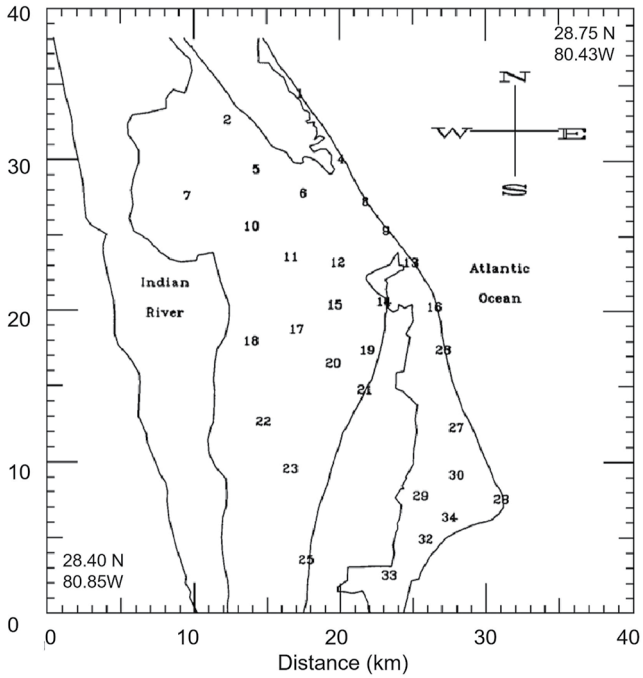

Figure 1. The Kennedy Space Center and Air Force Eastern Range field mill network (Launch Pad Lightning Warning System), including site IDs and locations. Typical separation distance between sensors is 2–4 km, with a few as large as 5 km.

with a digitizing resolution of 4 V/m, and the operating range was ±30 kV/m (Murphy, 1996). The devices were calibrated during manufacturing and are automatically calibration-tested each day by placing them in a calibration mode that applies known potential differences across the measurement plates. All field mills are mounted identically, and calibration in the field was carried out to address the impact of mounting geometry on the field magnitude. Previous studies by Jacobson and Krider (1976), Livingston and Krider (1978), Maier and Krider (1986), and Koshak and Krider (1989) have used these data to show the patterns of the PG and the changes in the PG produced by lightning near a variety of storms at the KSC-ER. These authors indicate that the field mill readings were generally accurate to within 10%. As we will show, an important advantage of the field mill network is its ability to sense the presence of an electrified cloud before the occurrence of any lightning discharges.

3.2. Cloud-To-Ground Lightning Surveillance System

At the time of this study, the CGLSS system was used to detect and locate CG flashes. This system contained five gated, wideband magnetic direction-finders similar to those described by Krider et al. (1980). These sensors were capable of locating the strike points of the first return strokes in CG flashes to within 0.5 km or better with a detection efficiency of at least 90% (Murphy et al., 1996; Wilson et al., 2009).

3.3. Lightning Detection and Ranging

The LDAR system was a total lightning (IC + CG) mapping system capable of detecting and mapping the locations of sources of VHF radiation that are produced by breakdown processes in both IC and CG flashes. Differences in time of arrival of VHF pulses were used to determine these source locations in three dimensions in a fashion similar to that described by Proctor (1971). The LDAR system used seven VHF receivers tuned to a frequency of 66 MHz with a bandwidth of 6 MHz, as described in detail in Lennon and Maier (1991). The LDAR system accuracy was tested by Maier, Lennon, Krehbiel, et al. (1995) and Maier, Lennon, Britt, and Schaefer (1995) using the known locations of a NASA test airplane fitted with a 66 MHz transmitter, and was further evaluated in detail by Boccippio et al. (2001a, 2001b). In these studies, it was determined that the average three-dimensional location error of the LDAR system was less than 0.5 km within 20 km of the central receiving site, and was less than 1 km for sources that were within 20–40 km of the central site. The estimated LDAR flash detection efficiency exceeded 95% within 50 km of the central site.

For this study, all flashes reported by CGLSS were presumed to be CG flashes. All flashes reported by the LDAR system that were not reported by CGLSS were presumed to be IC flashes. The behavior of fast potential gradient changes reported by the LPLWS was consistent with these presumptions.

3.4. NEXRAD

The Next Generation Weather Radar (NEXRAD) system is a network of 160 high-resolution S-band (10 cm wavelength) weather radars jointly operated by the National Weather Service (NWS), the Federal Aviation Administration (FAA), and the U.S. Air Force. At the time of this study, the NEXRAD system only reported precipitation-related products at various elevation angles depending on location and weather conditions, with volume scans every 5–6 min. Archived NEXRAD Level-II reflectivity products were obtained through the NOAA public S3 bucket on Amazon (https://noaa-nexrad-level2.s3.amazonaws.com). Radar reflectivity analyses were performed using smoothed GR2Analyst imagery (https://en.wikipedia.org/wiki/GRLevelX; https://grlevelxusers.com/faq/), in order to be consistent with Air Force launch weather operations at KSC. Unsmoothed reflectivity values were used to estimate the maximum reflectivity above the freezing level (0°C). Temperature heights were determined using information provided by the closest routine soundings at KSC (XMR) or

Table 1
Isolated Thunderstorms

Case ID	Storm date	Lightning interval (UTC)	First flash (UTC)	Closest EFM to storm center	Cell history	Propagation direction	Distance to closest cell (km)[a]	Distance to 2nd closest cell (km)[a]	Comments
1	11 June 1995	15:47–16:54	15:47:49.0	Site 12	Merged	SW	0.0	12.5	Two cells merged during initial electrification
2	23 July 1995	20:04–20:11	20:04:44.3	Site 12	Single	W	0.0	10.2	Used Tampa NEXRAD data; no lightning in prior 90 min
3	24 September 1995	20:00–20:33	20:00:15.0	Site 8	Single	NE	0.0	34.5	Second of three cells developing along coast and propagated sequentially off-shore
4	11 June 1996	18:12–18:27	18:12:13.4	Site 16	Merged	NE	0.0	NA	Two cells merge during init. electrification; Sites 12 and 13 not available
5	27 June 1997	16:58–17:13	16:59:28.9	Site 12	Single	Fixed	0.0	20.0	First cell of the day within the LPLWS network
6	08 July 1997	17:25–18:01	17:25:40.7	Site 23	Single	S	1.0	13.0	Widespread low-level moisture
7	15 July 1997	17:20–17:34	17:21:03.0	Site 22	Multi	Fixed	1.0	3.5	Weakening 2nd closest cell; an earlier cell produced elevated fair-Wx field at Site 17 at 16:55, but died-out
8	17 July 1997	17:40–17:45	17:40:42.8	Site 17	Multi	Fixed	0.2	4.6	Weakening 2nd cell died after 17:23
9	25 August 1997	15:50–16:40	15:50:34.9	Site 22	Seq.	S	0.0	13.5	Sequence (seq.) of cells. Electrified cell developed over site 18 and propagated to site 22 during initial electrification
10	05 August 1998	16:30–16:38	16:30:16.4	Site 29					No NEXRAD Available
11	10 July 1999	17:39–18:33	17:39:10.7	Site 15	Merged	Fixed	0.0	6.9	Earlier cell over Site 12 < 30 dBZ@−10°C; nearby 2nd cell weakened and merged
12	04 August 1999	04:27–05:28	04:27:22.2	Site 30	Single	Fixed	0.0	9.4	Multiple distant mature cells to the south, east, and west
13	23 June 2000	15:57–16:16	15:57:33.3	Site 21	Single	Fixed	0.0	13.0	Second cell was west of LPLWS network

[a]Horizontal distance between LPLWS site closest to the first flash and the closest 20 dBZ reflectivity value above the 0°C level.

Tampa (TBW) (http://weather.uwyo.edu/upperair/sounding.html) that were also closest in time before each case. Comparison of soundings when both sites were available showed very small (less than 300 m) differences in measured temperature heights.

4. Specific Events Analyzed

This section briefly describes the context, location, and timing for the thunderstorm cases that have been evaluated. Table 1 lists the 13 isolated thunderstorms that were selected for analysis together with details for each case. The cases were initially selected by reviewing video animations of the LDAR display and identifying times of the onset of lightning with no prior lightning within 10 km during the previous 30 min. Case selection was further refined using both surface potential gradient timeseries and NEXRAD reflectivity observations. The lightning interval started when the LDAR system detected the first lightning discharge, and stopped when the LDAR activity ceased. The "storm centers" were defined as the average location of the first five LDAR sources associated with each flash occurring during the initial 5 min of each storm, but this information is reflected in the table as the closest EFM site for easier interpretation. This definition of the storm center provides the location of the most electrically active portion of the cell at the time of first lightning. For the storm on 11 June 1996 (960611) the LDAR data were not available, so the storm center was defined as the average location of all CG flashes that occurred over a 10-min period starting when the first CG flash was detected.

The conditions leading to the first lightning in a cell are described from the perspective of the NEXRAD radar, which provides an objective means to identify storm development and motion. A "cell" was defined by vertically growing clouds that had a reflectivity greater than 20 dBZ above the freezing level (0°C). Table 1 also contains

Table 2
Long, Horizontal Flashes

Case ID	Date	Time (UTC)	Time since previous Ltg (min)	Distance to network (nm)	Propagation direction	Affected areas at the KSC-ER
1	13 June 1995	08:41:09.5	>60	35[b]	NE	Extreme SW
2	08 July 1995	00:25:46.1	11	40[b]	E	West central fringe
3	08 September 1995	22:02:30.2	38[a]	20	NW	Southern third
4	12 June 1996	02:37:35.7	49	55	NE	Southern quarter
5	15 June 1996	22:34:39.1	10	25	N	Entire network
6	18 September 1996	19:31:06.3	>60	30	SE	Western fringe
7	08 July 1997	22:16:29.7	12	35	NE	Entire network
8	08 July 1997	22:37:00.0	11	35	NE	Entire network
9	18 July 1997	22:33:11.7	21	10[b]	S	Entire network
10	18 July 1997	22:51:58.8	11	10[b]	S	Entire network
11	18 July 1997	23:12:36.4	21	10[b]	S	Entire network
12	04 August 1997	21:01:08.5	24	25[b]	W	Entire network
13	04 August 1997	21:27:07.9	26	25[b]	W	Southern 2/3

[a]Activity remained within 10 nmi of network perimeter until 9 min prior to flash. [b]Insufficient data to determine entire distance. Distance (Dist.) is the minimum possible value.

the distance between the closest LPLWS site and the lightning-producing cell (closest 20 dBZ cloud edge above the 0°C level), and to the next-closest cell during the time of initial electrification of the lightning-producing cell. A distance of zero in the table indicates that the closest LPLWS sites with within the 20 dBZ perimeter of the cell just prior to initial electrification. Note that two of the cases did not have nearby NEXRAD volume scans (Cases 2 and 10), although the TAMPA NEXRAD was able to provide limited information for Case 2. Out of the remaining 11 cases, 5 were isolated single cells, and 3 were cells that merged prior to or during initial electrification. For the three cases where the nearby "2nd cell" was closer than 9.4 km (Cases 7, 8, and 11 in Table 1), these second cells either died-out during initial electrification or became part of the cell of interest. Regarding cell movement, five of the cases involved cells that propagated in various directions, and six were stationary (fixed).

Table 2 shows dates for the 13 long, horizontal discharges that propagated into the KSC-ER and were subjected to detailed analysis. These flashes occurred on nine thunderstorm days and were initially screened using video tape recordings of real-time LDAR display. They were further analyzed using the source-level digital LDAR data. These LDAR cases together with LPLWS PG data for the same events were used to determine the time delay from the previous discharge and values of the PG before and after the flash. All 13 cases in Table 2 were flashes that were separated by at least 10 min from the previous discharge and extended at least 10 nmi from their point-of-origin outside of the field mill network to the perimeter of the network (Distance to Network in Table 2). It should be noted that the flash time was determined from the initial maximum slope in the PG seen in-common by most of the field mill sites.

5. Examples of Initial Electrification

Figure 2 shows the surface PG signatures under/near five isolated thunderstorms at the KSC-ER just prior to and after the initial lightning discharges. All records include the field mill site of the measurement as well as the distance from that site to the estimated storm center. We note that the subtle features in the timeseries plots that we describe below may be difficult to see in printed form. We have attempted to address this by limiting the number of waveforms in each plot within the body of the manuscript, and then providing a more-complete set of waveform plots in Supporting Information S1. We also note that determination of the onset of initial deflection of the electric field is difficult. In this work, we extrapolated back-in time from "Big-E" potential gradient values (greater than +500 V/m or less than −100 V/m), picking the time when the values became indistinguishable from the background noise level, while also considering observations from multiple nearby sites. Because of the

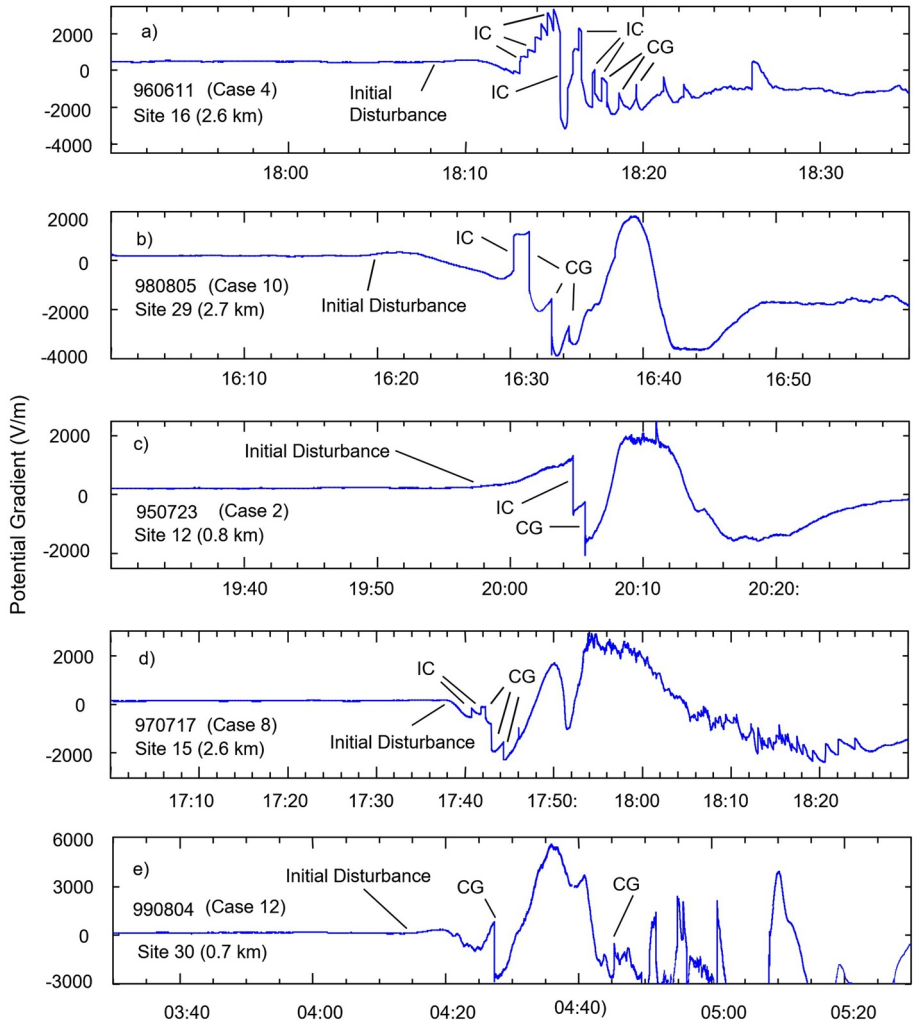

Figure 2. Potential gradient records before and during the initial electrification of five isolated thunderstorms showing the times of the initial field disturbances and the initial lightning discharges. Each panel includes the field mill numbers (IDs) where measurements were taken and the corresponding distances to the initial discharge location. Electric field records correspond to the following storm dates: (a) 11 June 1996; (b) 5 August 1998; (c) 23 July 1995; (d) 17 July 1997; (e) 4 August 1999.

uncertainty in these initial deflection times, we also recorded and analyzed the times of the first Big-E values noted above.

The storm of 960611 (Case 4—Figure 2a) shows a modest positive offset (initial disturbance) in the PG beginning around 18:08 UTC reaching a maximum value of +846 V/m, followed by a negative excursion reaching −173 V/m between 18:11 and 18:12 UTC. This pattern is consistent with the initial development of lower positive charge (LPC) during or before the development of a more-dominant region of negative charge at higher altitude as discussed by Murphy (1996). The influence of LPC on the surface PG showed an increase between 18:12 and 18:15 UTC associated with a series of six intracloud (IC) discharges. The surface field polarity reversed in Figure 2a subsequent to an IC discharge (likely between the main negative and the LPC region) shortly after 18:15 UTC. Additional IC discharges between 18:15 UTC and the first cloud-to-ground (CG) discharge (as reported by the CGLSS network) at 18:17:57 UTC produced additional polarity reversals. The creation of sustained PG offsets of both polarities by lightning is consistent with earlier findings discussed in Section 2.1 (Coleman et al., 2003; Holden et al., 1983; Jacobson & Krider, 1976; Mo et al., 2002). Note that the IC discharge just before the first CG flash increased the influence of LPC on the surface PG, and during the first CG flash this returned to the level seen just before that IC discharge.

The storm on 980805 (Case 10—Figure 2b) shows an initial positive PG disturbance at 16:20 UTC consistent with development of a LPC region, followed by stronger influence of negative charge aloft at higher altitudes starting at about 16:23 UTC. The first lightning flash occurred at 16:30:16 UTC and was an IC flash that reversed the polarity of the PG, a behavior consistent with significant LPC. The influence of this LPC was reduced, leading to a polarity reversal in the PG, during a CG discharge at 16:31:27 UTC, likely due an abrupt removal of significant lower positive charge by lightning (Jacobson & Krider, 1976). Subsequent CGs at 16:33:06 and 16:34:26 UTC may also show evidence of an enhanced LPC prior to their occurrence. Unlike Case 4 however, there was no evidence of neutralization of lower positive charge by IC discharges during this storm.

For the storm on 970717 (Case 8—Figure 2d), evidence for the creation of LPC prior to the first lightning discharge was weak or absent, in that the initial PG disturbance was negative beginning at 17:37 UTC. This is one of two (out of 13) cases that showed no evidence of initial development of lower positive charge. No EFM sites were directly beneath the cell, reducing the likelihood of detecting lower positive charge, but three sites were within 2.6 km of the storm center. Not until the first IC discharge at 17:40:43 UTC was there evidence of a LPC region, resulting in a small positive change in the surface PG. As in the prior two cases, the first CG flash at 17:42:17 UTC was preceded by a sustained positive PG associated with an IC discharge. The change in PG associated with this IC discharge likely reflects either an increased LPC region or a decreased mid-level negative charge region that "exposes" an existing LPC region.

The storm on 950723 (Case 2—Figure 2c) produced just one CG flash during the entire storm, and in contrast to our previous examples, there was no evidence of negative charge at the surface prior to the first discharge. A positive disturbance in PG starting at 19:57 UTC dominated the pattern until the first IC discharge occurred at 20:04:44 UTC, and that discharge reversed the field polarity, likely by reducing LPC. The first IC flash was followed by a period of modest positive PG recovery prior to the one and only CG discharge at 20:05:38 UTC.

Our last example is the storm on 990804 (Case 12—Figure 2e) that began at 04:15 UTC with an initial positive disturbance and, like most other cases, this was followed by a negative trend indicating dominant negative charge shortly after 04:20 UTC. Unlike all other cases, the first lightning discharge was a CG at 04:27:22 UTC. As in the other cases, this CG discharge was preceded by the appearance of increasing positive PG excursion, likely reflecting development of LPC prior to its occurrence. It should be noted that there was heavy rainfall at this site beginning at 04:21 UTC, and this may have created the later local "agitation" of the PG.

These representative cases suggest that lower positive charge in developing isolated Florida storms is affecting the surface PG before more-distant (higher altitude) negative charge develops sufficiently to dominate the surface PG.

6. Initial Electrification as a Function of Distance to Early Lightning

Figures 3–7 show each of the five storms discussed above in more detail, organized as three-panel figures for each case. The primary image in the top-left panels (a) show a Plan Position Indicator (PPI) view of the NEXRAD radar reflectivity for a single elevation angle (tilt) near the 0°C level, closest in time to the initial PG disturbance. In these figures, the NEXRAD site in Melbourne FL (KMLB) was used unless noted otherwise. The "storm center" (early lightning, as defined in Section 4) is at the center of the white case ID surrounded by a black circle in these images. An inset image in this panel shows the radar reflectivity cross-section along the white line on the PPI panel. The map in the upper-right panels (b) show the locations of CG flashes near the time of storm development (generally the first 30–60 min of CG activity), as well as the location of the first CG flash. The PGs records for the three closest sites to the storm center are given in the lower panels (c through e). As was the case for Figure 2, all records contain the site number where measurements were taken as well as the distance from that site to the LDAR-derived storm center. The gray region in these records indicates the time period for the radar volume scan shown in panel (a).

The storm on 960611 (Case 4—Figure 3) was a small cell that started to develop close to Sites 12 and 14, and then moved NE toward Site 13 and into the Atlantic Ocean. EFM sites 12 and 13 were not operating for this case, so Site 16 was the closest available site to the storm center. A simultaneously developing cell merged with this cell between 18:02 and 18:07 UTC. Near the time of initial disturbance in PG, reflectivity exceeded 40 dBZ between the freezing level (0°C at 14.4 kft) and the −10°C temperature height (21.3 kft), falling to below 30 dBZ above the −20°C height (25.2 kft). This storm showed an initial positive PG disturbance at the three closest sites (Figures 3c–3e) but was not the largest at the closest site. Evidence of an initial positive excursion was weaker

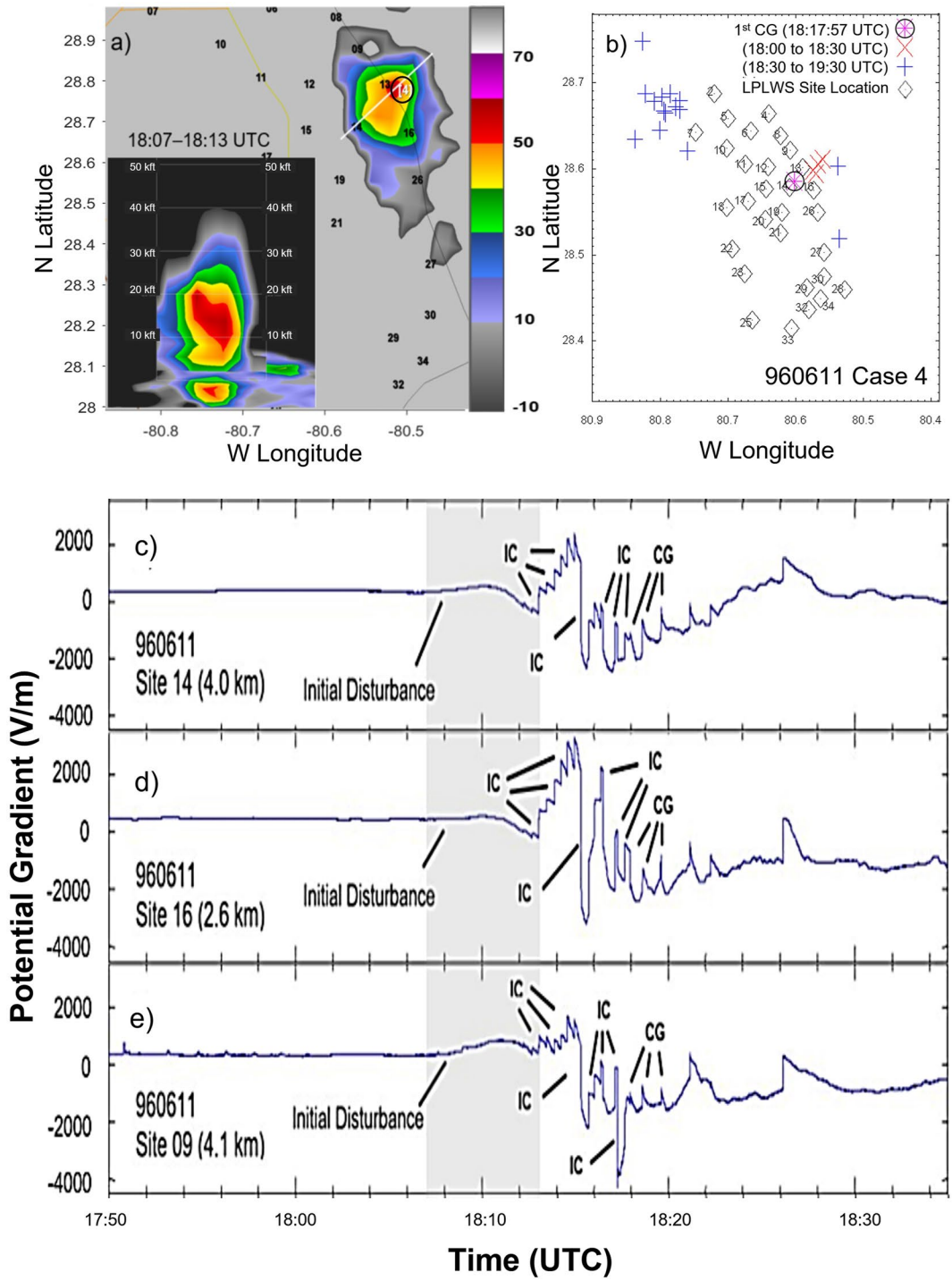

Figure 3. Radar reflectivity, lightning locations, and nearest surface potential gradient (PG) waveforms for Case 4 on 11 June 1996. (a) Plan Position Indicator (PPI) view of radar reflectivity for tilt near the freezing level, nearest to the time of the initial PG deflection. Case ID in brackets and circled in black is the "storm center" (first flashes). Inset image in this panel is the radar reflectivity cross-section along the white line on the PPI image. (b) Locations of cloud-to-ground lightning at times indicated in the legend. (c–e) PG recorded at the three sites closest to the storm center. All field records contain the site ID where measurements were taken as well as the distance from that site to the Lightning Detection and Ranging-derived storm center. The gray region in these field records indicates the time period for the radar volume scan shown in panel (a).

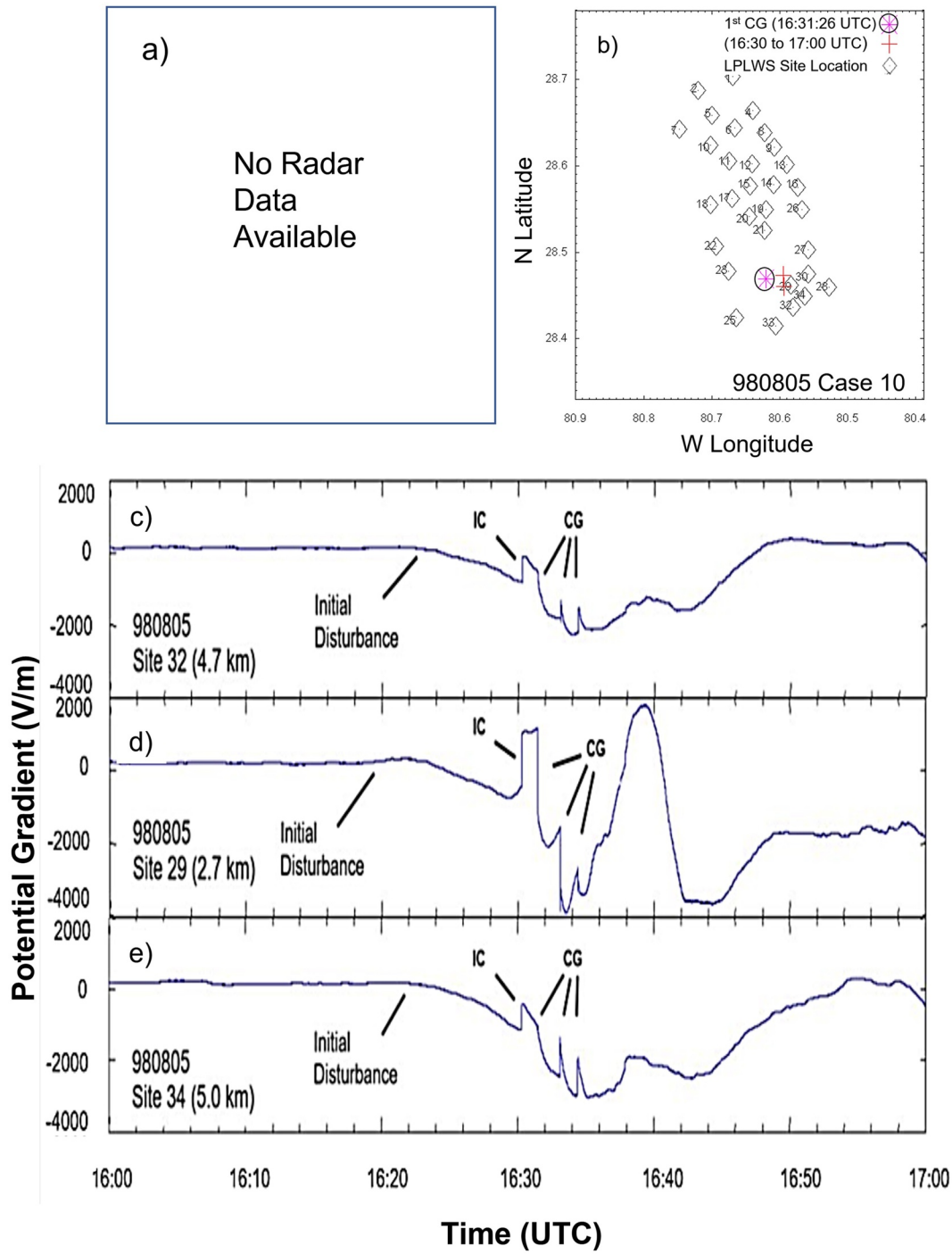

Figure 4. Lightning locations and nearest surface potential gradient waveforms for Case 10 on 5 August 1998, organized as in Figure 3. Radar data were not available for this case.

further away at Site 08 and visually non-existent at Site 26 (shown in Figure S1 in Supporting Information S1). The initial electrification was detectable several minutes prior to the first lightning discharge at the three closest sites. All sites showed evidence of a growing negative charge center during the minute before the first lightning discharge, as evidenced by the negative trend in the surface PG.

The small storm on 980805 (Case 10—Figure 4) featured an initial positive PG deflection at site 29 closest to the storm center (2.7 km—Figure 4d), but this feature was not as clear for all other sites a few kilometers further

away from the storm center (see Figures 4c and 4e). In contrast, negative field excursions were present at all nearby sites prior to the initial lightning discharge (IC) at 16:30:16 UTC and these excursions had similar timing across the measuring sites, suggesting that the mid-level negative charge region might be spatially larger and/or more homogeneous than the LPC region (see Figure S2 in Supporting Information S1 for the five closest sites). Note that after the initial IC discharge at 16:30:16 UTC, only the closest site had clear evidence of dominant LPC (a positive surface PG) prior to the first CG flash at 16:31:27 UTC. The related field changes at the other sites could (alternatively) be explained by removal of negative charge by the IC flash. As noted in Table 1, no radar data were available for this case.

The storm on 950723 (Case 2—Figure 5) produced just a few flashes, and only the second flash was CG. The initial PG disturbance was positive and large at sites 11 and 12, and was largest at the nearest site (Site 12). There were no large excursions (>+500 V/m) prior to the initial IC discharge at 20:04:44 UTC except for Sites 09 and 12 (see Figure S3 in Supporting Information S1 for the five closest sites). Interestingly, the most-distant of the closest five sites (Site 11—Figure 5e) exhibited the second largest positive PG excursion before the first flash. KMLB NEXRAD data were not available for this case, so the Tampa NEXRAD site was used. The lowest tilt for this radar was for reflectivity at about 12 kft for this storm, given its long distance to the cell (>190 km). Sites 12 and 11 were near the edges of this cell (Figure 5a) and were the sites that showed large, slowly developing positive excursions in PG beginning roughly 6–10 min prior to the first lightning discharge. This spatial variability of the initial disturbance in PG again supports the high variability (small and non-uniform nature) of the LPC regions. The wide variation of initial disturbance times is consistent with the findings of Murphy (1996).

In contrast, the storm on 970717 (Case 8—Figure 6) had no clear evidence of an initial positive PG disturbance. Figures 6c–6e show that the initial PG disturbances was predominately negative at the nearby field mill sites, and these negative excursions were not as sensitive to the storm distance as the initial positive disturbances seen in previous storm cases (see Figure S4 in Supporting Information S1 for the five nearest sites). It is worth noting that this was one of three cases where the closest EFM was outside of the 20 dBZ reflectivity boundary of the cell (see Table 1), with a minimum distance from the storm center of 2.3 km. The initial negative disturbance was detectable only about 4 min before the first lightning flash at all locations. The radar volume scan during the 5 min leading up to the initial negative deflection (Figure 6a) shows the coldest portion of the cell being closest to Site 11, with 0 dBZ reaching 30 kft and 30 dBZ reaching above 25 kft (−20°C).

The storm on 990804 (Case 12—Figure 7) behaved similarly to Cases 4 and 10 (Figures 3 and 4, respectively) in that the initial PG disturbance at the closest site (Site 30—Figure 7d) was positive, followed by a negative excursion before the first lightning flash which was a CG. The positive disturbance starting at about 04:15 UTC was weak at more-distant sites, and was absent furthest away from the cell at Site 27 (Figure 7e). A negative excursion was evident at all sites beginning around 04:20 UTC before the first flash (see Figure S5 in Supporting Information S1 for the five nearest sensors). The initial storm-related field disturbances were evident about 12 min prior to the first flash at the closest site (Figure 7d) and was delayed and inverted further away at Site 27 (Figure 7e). It should be noted that heavy rainfall began just after 04:20 UTC at Sites 29 and 30 and may have disturbed the fields at those sites after that time.

The findings reported in this section suggest that during initial electrification of these storms, LPC may be less uniform than mid-level negative charge, and is likely smaller in spatial extent. They also show that positive initial deflections are seen before negative excursions when they both occur. Also, the maximum in surface positive PG before the first flash was not always seen closest to the storm center (initial flash location) but was always within about 4 km of it. These observations are further supported in the analyses of all 13 cases provided below.

7. Values of PG Associated With the Initial Electrification

Specific values of the maximum and minimum PG at the surface before the onset of lightning are discussed here in the context of the Natural and Triggered Lightning Launch Commit Criteria (LLCC). The rule for developing cumulus clouds that have not yet produced lightning (NASA-STD-4010, 2017, Section 4.1.3) states that:

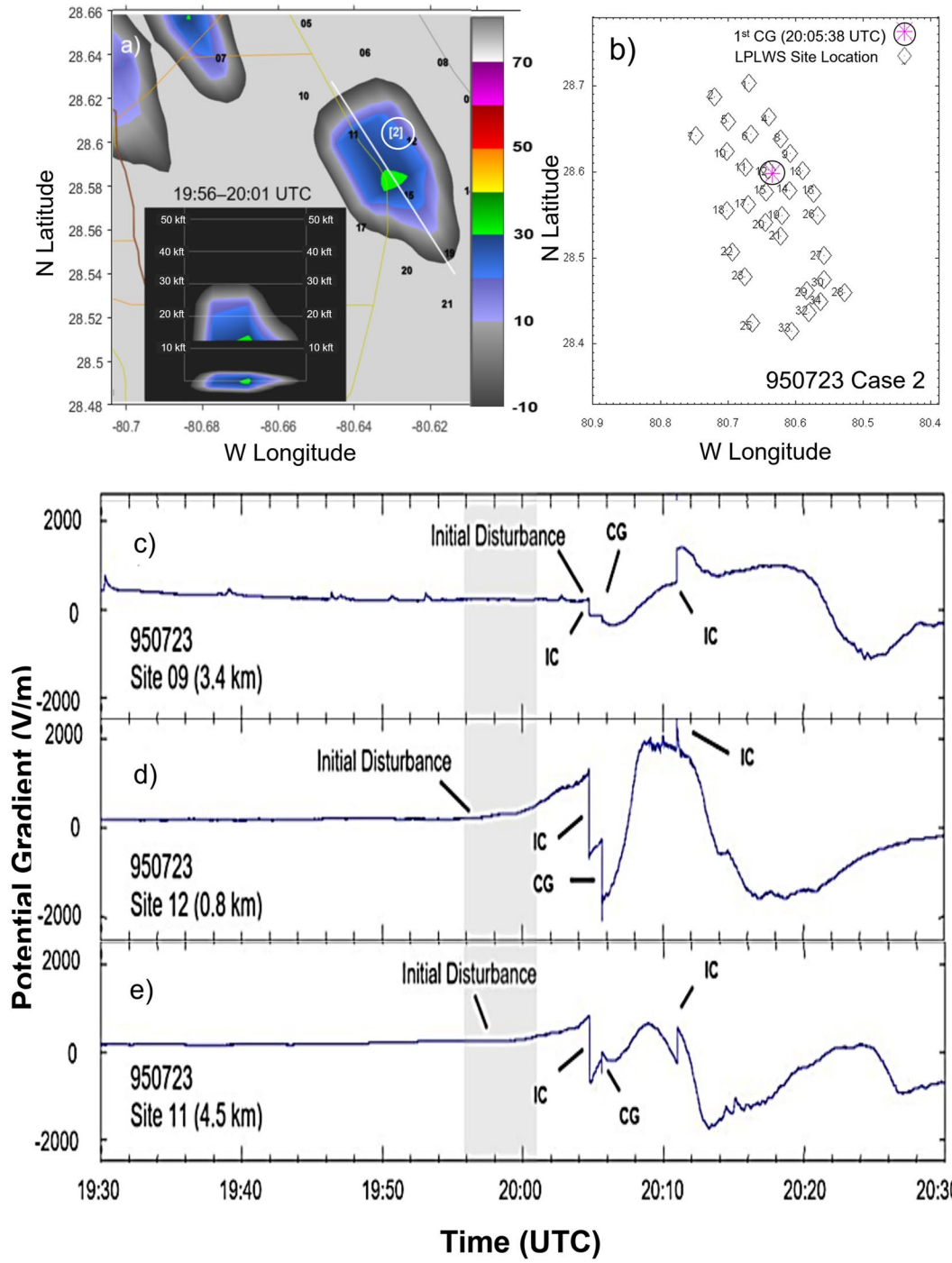

Figure 5. Radar reflectivity, lightning locations, and nearest surface potential gradient waveforms for Case 2 on 23 July 1995, organized as in Figure 3. (a) Plan Position Indicator view of radar reflectivity for lowest tilt for KTBX (Tampa), nearest to the time of the initial potential gradient deflection.

Flight path through the cloud: A launch operator shall not launch if the flight path will carry the launch vehicle through any cumulus cloud if either of the following conditions applies:

1. The cloud has a top at an altitude where the temperature is colder than or equal to +5°C and warmer than −5°C unless:

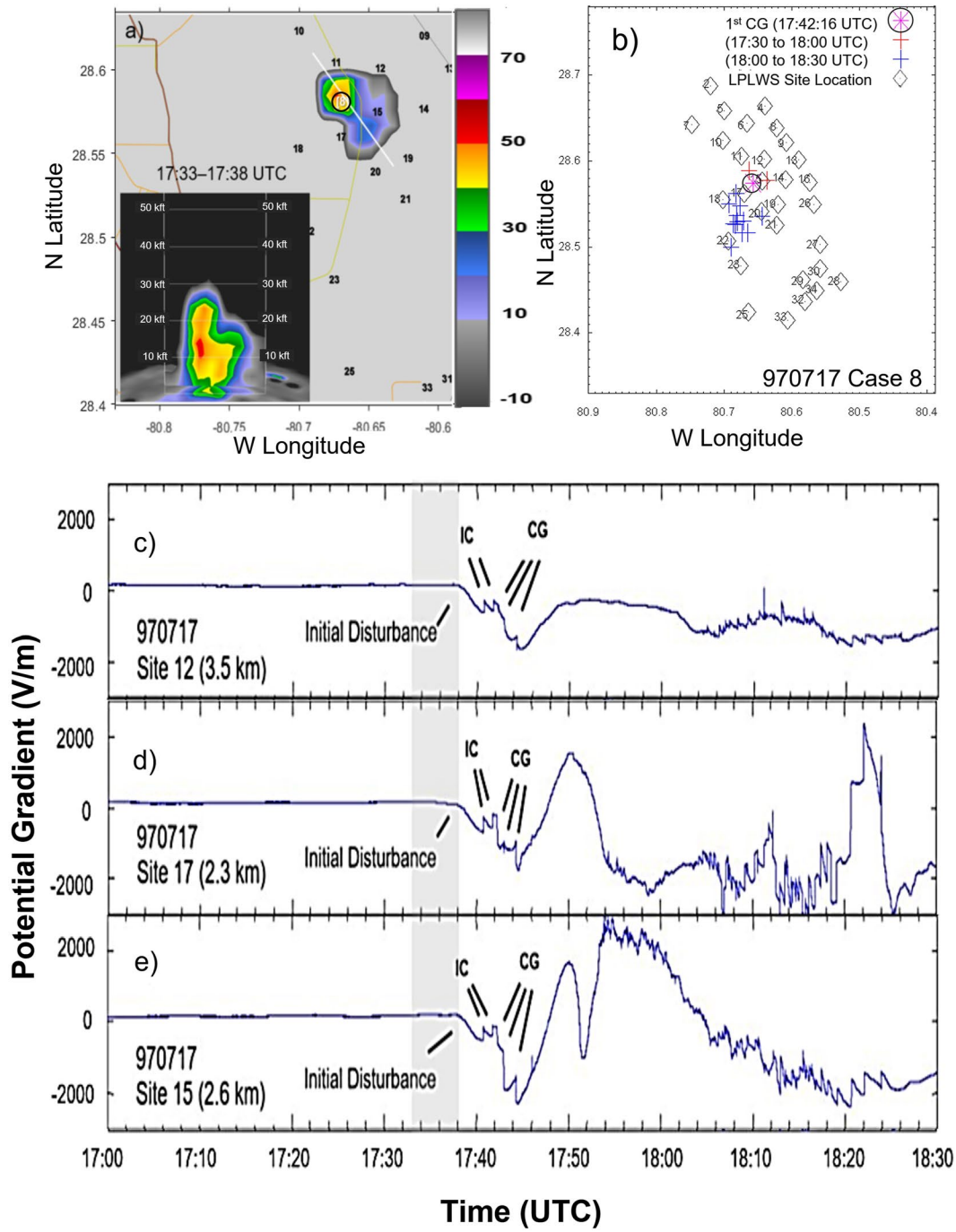

Figure 6. Radar reflectivity, lightning locations, and nearest surface potential gradient waveforms for Case 8 on 17 July 1997, organized as in Figure 3.

- The cloud is not producing precipitation;

AND

- The horizontal distance from the center of the cloud top to at least one working field mill is less than 2 nmi;

AND

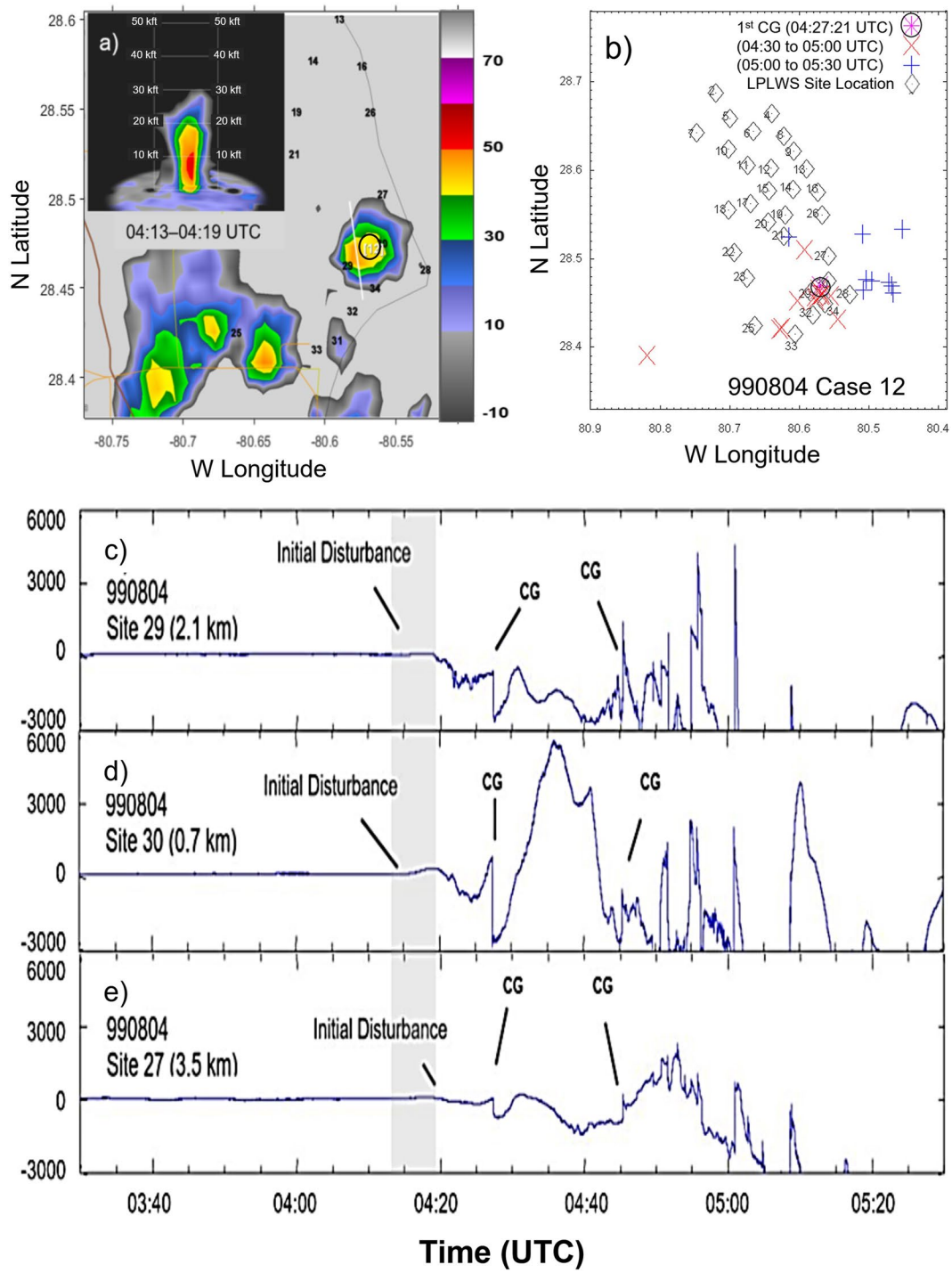

Figure 7. Radar reflectivity, lightning locations, and nearest surface potential gradient waveforms for Case 12 on 4 August 1999, organized as in Figure 3.

- All electric field measurements at a horizontal distance of less than or equal to 5 nmi from the flight path, and at each field mill specified in Section 4.1.3.1a(2) in this NASA Technical Standard, have been between −100 and +500 V m^{-1} for at least 15 min;

OR

2. The cloud has a top at an altitude where the temperature is colder than or equal to −5°C.

Table 3
Values of Potential Gradient Before the First Lightning at the Kennedy Space Center and Air Force Eastern Range

Case ID	Storm date	PG maximum (V/m)	PG minimum (V/m)	Closest sites below −100 V/m	Closest sites above +500 V/m	# Sites <10 km	#Sites <10 km in violation
1	11 June 1995	+711	+81	0	2	18	5
2	23 July 1995	+1,261	+174	0	2	16	2
3	24 September 1995	+3,902	+11	0	5	15	6
4	11 June 1996	+846	−173	1	4	13	8
5	27 June 1997	+757	+152	0	2	18	2
6	08 July 1997	+141	−377	4	0	12	8
7	15 July 1997	+207	−322	4	0	11	5
8	17 July 1997	+197	−698	5	0	18	10
9	25 August 1997	+249	−2,599	5	0	8	8
10	05 August 1998	+333	−1,221	5	0	14	14
11	10 July 1999	+121	−1,485	5	0	17	13
12	04 August 1999	+614	−1,299	4	1	9	5
13	23 June 2000	+737	−24	0	1	16	1

On the face of it, these 0 dBZ cloud top constraints may seem overly cautious. Several factors contribute to these conservative constraints. First, given the high cost of failure during launch (safety and equipment), the LLCC targets a "one-in-ten-thousand" chance of lightning attachment or triggering, when quantification is practical. Additionally, there is uncertainty in the timeliness and accuracy of all meteorological observations, from aircraft or radar-based estimates of cloud height to surface electric field measurements, to the location and extent of lightning channels. Finally, there are gaps and imperfections in our understanding of cloud electrification and decay, and their relationships to precipitation aloft. All of this leads to conservative launch rules that derive more from the perspective of "this has been shown to happen" and "this could happen," as opposed to a balance between false-alarm rate (FAR) and failure-to-warn. For these reasons, this study was not designed to include estimates of FAR, but rather to search for challenging cases and look for the worst-case outcomes.

In order to evaluate the effectiveness of cumulus rule listed above, Table 3 provides the maximum and minimum PGs that were detected at the five closest field mill sites in the 15-min interval before the first lightning flash (IC or CG). Table 3 also includes the number of field mill sites (among the five closest) that exceeded the −100 and +500 V/m thresholds stated in the LLCC. To explore the spatial extent of elevated surface PGs, the table also includes the number of sites that were within 10 km of the storm center (defined in Section 4), and the number of these sites with maximum or minimum potential gradients that violated a PG threshold during the 15-min intervals.

Table 3 shows that the LLCC for cumulus clouds given in this section did provide warnings prior to the occurrence of the first lightning in all 13 storms that were analyzed. However, four cases (Cases 1, 2, 5, and 13) were dangerously close to not being detected because threshold PG values were only exceeded at one or two sites. Increasing the time interval from 15 to 30 min prior to the first flash made no difference in the number of closest sites that violated the LLCC (not shown).

It should be noted that interference from prior or developing storm cells may have increased the number of sites in violation within 10 km for some of the cases (e.g., Cases 8–11) but would not have impacted the closest five sites due to the distances involved (see Table 1).

8. Initial PG Disturbance and Radar Reflectivity Relative to Times of Initial Discharges

Operationally, a significant question in the warning of a possible lightning hazard is the lead time provided by the field mill network relative to selected radar parameters. As discussed in Section 2.4, numerous studies have evaluated lead-times (before lightning) using radar-based parameters, but only a few have compared simultaneous

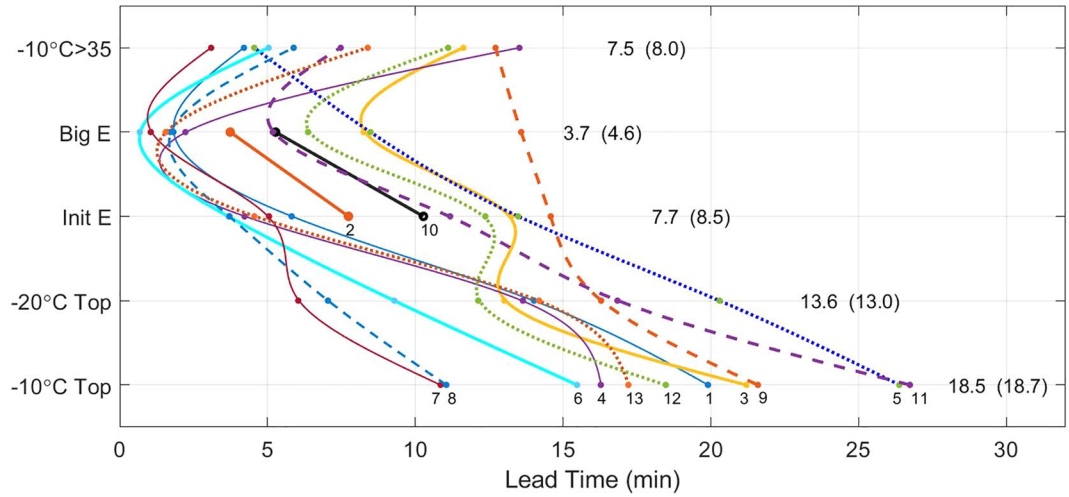

Figure 8. Summary of lead-time before first lightning flash for potential gradient (PG) and radar parameters. The lead-time profiles are for 13 isolated cells at the Kennedy Space Center and Air Force Eastern Range. Case numbers are noted along the bottom of the panel, and median (mean) lead-times for each parameter are shown to the right of the curves. The "Tops" are for 0 dBZ reflectivity at the specified temperature heights. "Init E" occurs at the earlier PG deflection from the baseline fair-weather value. "Big E" occurs when the PG is more-negative than −100 V/m or more-positive that +500 V/m.

radar and surface PG measurements. Here we provide lead-time assessments for our 13 cases of isolated thunderstorms at the KSC-ER using the following NEXRAD radar and surface PG parameters:

- −10°C Radar Cloud Top (0 dBZ).
- −20°C Radar Cloud Top (0 dBZ).
- >35 dBZ radar reflectivity above −10°C ("Reflectivity:Height Radar Metric").
- Initial PG Disturbance (Init-E).
- LLCC Threshold PG (<−100 or >+500 V/m) (Big-E).

Given the long time required to complete the radar volume scans (5–6 min), the times for the radar parameters listed above (for the 11 cases with radar observations) were computed using linear interpolation between the related tilt times for volume scans prior to and following the condition. In addition, maximum radar reflectivity above the freezing level (MRR) values were computed using the volume scan just prior to Init-E and Big-E, defined as the maximum reflectivity above the 0°C level within the cell. This parameter is employed in the LLCC as a means to remove launch constraints under some conditions.

The findings from this study are shown in Figures 8 and 9, and Table 4. Figure 8 shows "profiles" of lead time for each case, for each of the five parameters listed above. Measured/computed values are small "dots" that are connected by smooth lines of the same color to facilitate viewing. Case numbers are noted along the bottom of the panel, and median (mean) lead times for each parameter (aggregated over all cases) are shown to the right of the curves. Cases without radar data (Cases 2 and 10) are identified by the short black and orange straight-line segments between Init-E and Big-E values. Parameters are "ordered" from (nominally) the largest to the least lead time (bottom to top), with the exception that the "Reflectivity:Height Radar Metric" was placed at the top to facilitate visual interpretation. Figure 8 shows that the −10°C top led the first lightning by at least 11 min, and by up to 27 min. In all but two cases (3 and 12), the −20°C top led initial electrification (Init-E) by a few minutes, and it always led Big-E by at least 5 min. Big-E always led the first lightning, but frequently only by 1–2 min. The "Reflectivity:Height Radar Metric" (>35 dBZ above −10°C) exhibited a wide range of lead times (3–14 min), sometimes occurring close to the time when reflectivity exceeded 0 dBZ at −20°C (−20°C Top).

Histograms for various parameters are provided in Figure 9. The maximum reflectivity above 0°C (MRR) at the time of initial deflection (Init-E) and the time when the PG was >500 or <−100 V/m (Big-E) were always above 30 dBZ and were significantly larger for Big-E (Figure 9a). Figure 9b shows the distribution of lead times of 0 dBZ cloud tops (−10 and −20°C) before initial electrification. The lead time of Init-E before Big-E is shown in Figure 9c, ranging between 1 and 6 min. There were large variations in lead times for −10°C above 35 dBZ

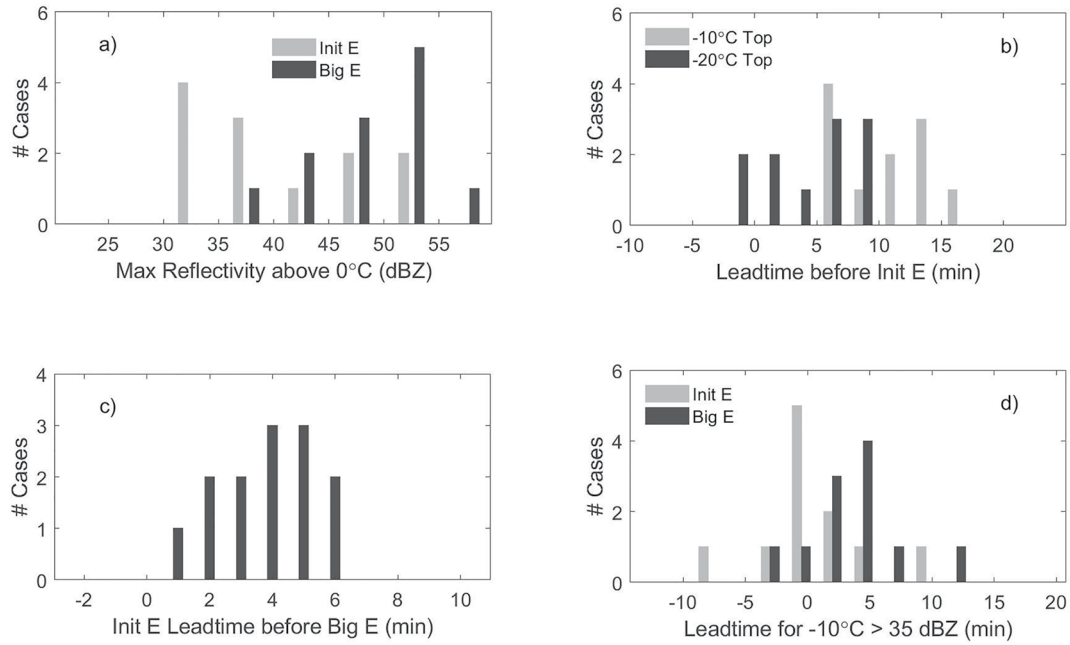

Figure 9. Lead-times and maximum reflectivity histograms for 13 isolated cells at the Kennedy Space Center and Air Force Eastern Range. (a) Histograms showing maximum reflectivity above 0°C at the time of initial deflection (Init E) and potential gradient values >500 or <−100 V/m (Big E); (b) Histograms showing lead time of 0 dBZ cloud tops (−10 and −20°C) before initial electrification; (c) Histogram of Init E before Big E; (d) Histograms of lead time for 35 dBZ at −10°C, relative to Init E and Big E.

before elevated PGs, showing lags (negative values) for a few cases (Figure 9d). Both Init-E and Big-E occurred before the 35 dBZ level was reached for Case 5, with Init-E leading by 9 min. Review of this case showed a nearly stationary cell developing over Site 9 with reflectivity reaching 25 dBZ at −10°C at the time of the initial PG disturbance (with fair-weather polarity). During the next radar volume scan, the cell showed evidence of decay that recovered and grew strong during the subsequent volume scan, exceeding 35 dBZ above the −10°C level. This interesting case clearly shows that initial electrification can occur well before a reflectivity of 30 dBZ reaches the −10°C level.

Table 4
Relative Times of Initial Potential Gradient Disturbance and Lightning Flashes

Case ID	Storm date	Big-E time (UTC)	Polarity (big-E/init-E)	Initial disturbance lag (min)	First flash lag (min)	First CG lag (min)	First CG after 1st flash lag (min)
1	11 June 1995	15:46	+/+	−4.0	1.8	4.5	2.7
2	23 July 1995	20:01	+/+	−4.0	3.7	4.6	0.9
3	24 September 1995	19:52	+/+	−5.0	8.2	32.4	24.1
4	11 June 1996	18:10	+/+	−2.0	2.2	7.9	5.7
5	27 June 1997	16:51	+/+	−5.0	8.5	10.6	2.1
6	08 July 1997	17:25	−/−	−3.0	0.7	5.0	4.3
7	15 July 1997	17:20	−/+	−4.0	1.1	2.2	1.2
8	17 July 1997	17:39	−/−	−2.0	1.7	3.3	1.6
9	25 August 1997	15:37	−/+	−1.0	13.6	17.8	4.2
10	05 August 1998	16:25	−/+	−5.0	5.3	6.5	1.2
11	10 July 1999	17:34	−/+	−6.0	5.2	10.9	5.7
12	04 August 1999	4:21	−/+	−6.0	6.4	6.4	0.0
13	23 June 2000	15:56	+/+	−3.0	1.6	5.7	4.1

Table 4 shows the lead times of the initial PG disturbance (positive slope in all but two cases), and lag times of the first flash (typically IC), all relative to the time of the first "Big-E" values. In each case, the time of the initial PG disturbance represents the earliest warning using surface PG observations that is possible prior to the first lightning discharge. Similarly, the times of the first flashes (typically IC) represent the earliest warning for CG lightning that would be provided by a total lightning mapping system.

Table 4 shows that for these 13 cases, the Big-E PG threshold interval (<−100 or >+500 V/m) was reached roughly 1–14 min before the first lightning discharge, with an extra few minutes provided by the onset time of the initial disturbance. While Init-E was positive in all but two cases, Big-E was positive in only 6 of the 13 cases. It is worth noting that the two cases with negative initial deflections (Cases 6 and 8—see Polarity column in Table 4) exhibited two of the four shortest lead-times for first flash (0.7 and 1.7 min). This may reflect a "masking" of the initial electrification because of canceling of the surface PG by lower positive charge. It should also be noted that sometimes it was difficult to select the time of the initial field disturbance, so it may not be a reliable metric for warning. Operationally, this uncertainty can be caused by interference from distant storms, the presence of non-thundery clouds that altered the fair-weather field profile, rain, and nearby surf electrification for coastal sites, among other factors.

As was noted above, IC discharges tended to precede the first CG flash by several minutes. In Case 3, there was a 24-min delay between the first IC and the first CG flash; however, in this case, there was also some uncertainty about whether the discharges originated from the same cell. It is also worth noting that for Case 12, the first discharge was a CG flash.

In Summary, the results shown in Figures 8 and 9, and Table 4, show that modest PG values (Big-E) were typically detected several minutes prior to the first lightning discharge. Earlier warning was frequently provided by the initial deflection (Init-E), but this may be difficult to identify in real-time. If these cases are representative of the spectrum of conditions at the KSC-ER, then it seems that radar reflectivity above the −10°C level (both 0 and 35 dBZ) are important supplements to surface measurements of PG if safety is the primary objective.

An important question related to lightning triggering by launch vehicles is the degree of cloud electrification (i.e., the field magnitude and vertical extent) before a developing cumulus cloud becomes capable of producing triggered lightning. Inspection of Figure 8 provides some insight into this question. There were two cases (03 and 12) where the initial deflection (Init-E) that warned of a more-significant PG (Big-E) occurred before the 0 dBZ cloud top reached an altitude of −20°C. Note that in these two cases, the 35 dBZ reflectivity had not reached the −10°C level before initial deflection in PG. Additionally, there were two other cases where Init-E occurred within 7 min of the cloud tops reaching the −10°C level (Cases 07 and 09). Given that a surface measurement of PG below vertically stacked charges, by its very nature, can only underestimate the onset and degree of charge separation aloft (due to partial cancellation of positive and negative fields at the ground), it is reasonable to suspect elevated fields in the cloud prior to having evidence on the ground. These findings and related inferences indicate that launch through a growing cumulus cloud with a 0 dBZ top above −10°C cannot be assumed safe.

9. Electric Fields and Radar Reflectivity Before and During the Propagation of Long, Horizontal Lightning

As was the case for initial electrification discussed above, there are surface potential gradient (PG) and radar reflectivity constraints employed in the LLCC to help assure launch safety during the conditions that lead to long horizontal flashes. Such flashes typically occur in attached and detached anvils associated with deep convection, and trailing stratiform regions behind convective lines—see Section 2.5. These same cloud regions are likely to have high internal electric fields that could result in lightning triggering by a launch vehicle passing through the region.

In the absence of recent lightning in or near an anvil cloud, the LLCC relaxes its constraint on flight through or near anvils if the MRR is less than 7.5 dBZ near the flight path. For detached anvils, an alternative way to relax the constraint for flight within 3 nmi of the cloud edge is for the following three conditions to exist:

1. No lightning within the detached anvil over the past 30 min; and
2. The absolute value of all surface PG measurements near the flight path have been less than 1,000 V/m for at least 15 min; and

Table 5
Surface Potential Gradient and Max Radar Reflectivity Prior to Long Horizontal Flashes

Case ID	Date	Time (UTC)	Maximum reflectivity above 0°C (dBZ)	Maximum PG (V/m)	Minimum PG (V/m)	Number of valid sites	Number of sites not in violation (all/flash)
1	13 June 1995	08:41:09	20–25	2,315	−4,244	28	10/0
2	08 July 1995	00:25:46	24–29	4,877	1,117	31	0/0
3	08 September 1995	22:02:30	22–27	7,039	−6,176	31	6/4
4	12 June 1996	02:37:36	24–30	2,075	−5,447	29	8/1
5	15 June 1996	22:34:39	22–29	7,095	−3,983	28	3/3
6	18 September 1996	19:31:06	20–28	3,336	1,162	29	0/0
7	08 July 1997	22:16:30	24–30	5,322	−4,011	31	7/7
8	08 July 1997	22:37:00	25–30	7,176	−2,403	31	2/2
9	18 July 1997	22:33:12	20–30	4,476	−5,366	31	3/3
10	18 July 1997	22:51:59	29–35	2,971	−5,369	31	7/6
11	18 July 1997	23:12:36	28–40	6,064	−2,897	31	4/2
12	04 August 1997	21:01:09	21–30	7,842	−1,430	31	1/1
13	04 August 1997	21:27:08	24–35	6,899	−2,368	31	1/1

3. The largest radar reflectivity from any part of the detached anvil cloud at a slant distance of less than or equal to 5 nmi from the flight path has been less than +10 dBZ for at least 15 min.

Our specific objective in this work is to study cases where long horizontal flashes occurred at least 10 min after the last flash to confirm that the vertical reflectivity profile and nearby surface PG values were consistent with the constraints listed above. A detailed study of the reflectivity and electrical structures of anvil and stratiform clouds prior to long horizontal flashes is beyond the scope of this work.

Here we look at the surface PG and maximum reflectivity above the 0°C level (MRR) just prior to the occurrence of long horizontal flashes, in selected regions where these flashes propagate (see Table 5). The range of MRR values for each case reflects the range of maximum values measured along the selected reflectivity cross-section. Table 5 also shows the maximum and minimum values of the PGs measured anywhere in the network, just before long, horizontal flashes propagated over the KSC-ER. It also shows the number of sites that had PG magnitudes less than 1,000 V/m prior to the event (i.e., sites that were NOT violating the LLCC) for all sites and for those within the flash area/extent. The pre-flash values are a 3-s average ending 0.5 s before the maximum slope of the lightning field change, in order to have a representative measurement just before flash initiation.

Table 5 shows that the 1,000 V/m threshold was violated in all 13 cases at a majority of field mill sites, supporting the underlying assumption that the LPLWS provides warning for such events. However, since the above values are only a snapshot of the potential gradient immediately before the discharge, the results should not be used to infer how long before the flash the field was elevated. Also, it should be noted that in 10 of the 13 cases, at least one site within the flash extent/area was not in violation of the LLCC threshold. Therefore, a single field mill will not provide adequate warning of large, horizontal discharge propagating into the area.

To gain more insight into the spatial pattern of surface PG at the time of horizontal flashes, Figures 10–18 show the areas affected by each flash together with the potential gradients before and after the discharge at all operational sites. The shaded regions show the area covered by the flash as reported by LDAR. These regions were drawn by hand, and only include regions having multiple LDAR source in close proximity. Spatially isolated LDAR sources were excluded as potential "outliers." The top and bottom numbers next to each field mill site give the pre- and post-flash values of the PG in volts per meter, respectively. The post-flash values are a 3-s average, beginning 0.5 s after the end of the flash. Six of these figures (Figures 10–15) also include supporting NEXRAD reflectivity information. The upper-right panels in these figures show PPI reflectivity for the tilt closest to the 0°C level just preceding the flash. The lower-right panels provide a vertical cross-section of reflectivity along

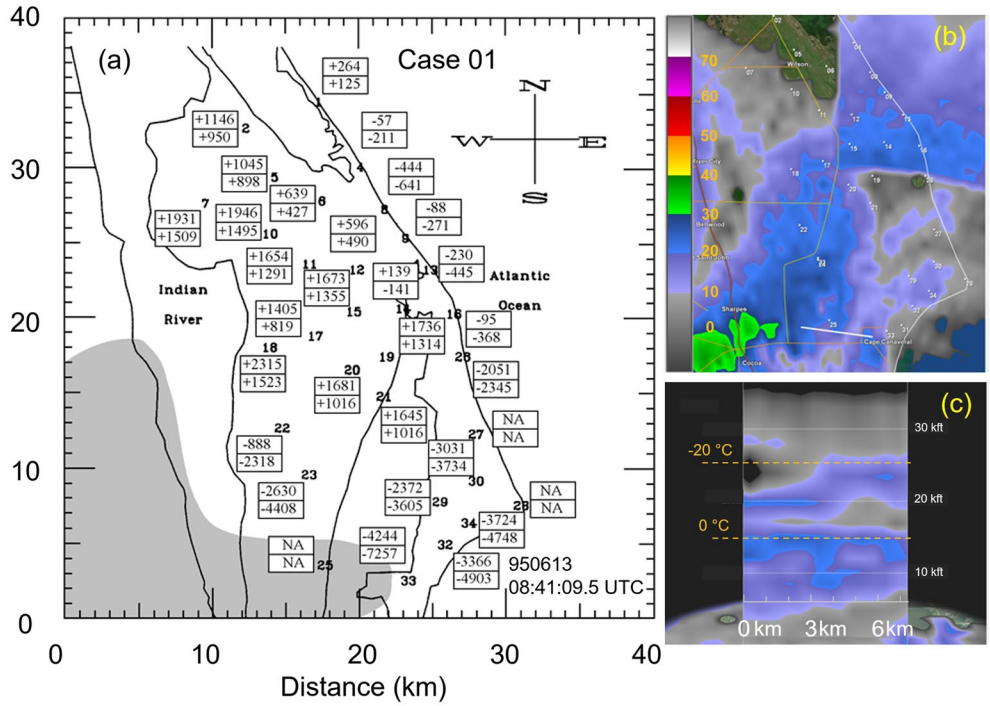

Figure 10. Radar reflectivity, flash envelope, and surface potential gradient (PG) for the long horizontal flash Case 1 on 13 June 1995. (a) PG values immediately prior to (upper value) and subsequent to (lower value) the flash are adjacent to the corresponding site ID. The shaded area represents the approximate aerial coverage (extent) of the flash. (b) Plan Position Indicator (PPI) view of radar reflectivity for tilt near the freezing level, nearest to the time of the flash. (c) Radar reflectivity cross-section along the white line on the PPI image, including approximate 0 and −20°C temperature heights.

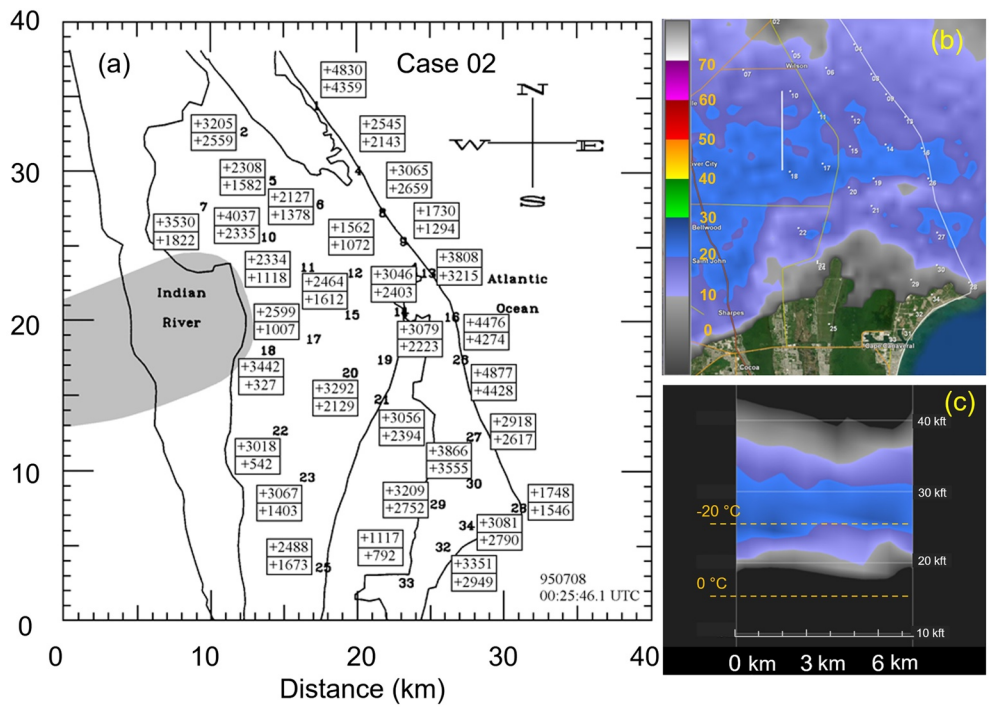

Figure 11. Radar reflectivity, flash envelope, and surface potential gradient for the long horizontal flash Case 2 on 8 July 1995, organized as in Figure 10.

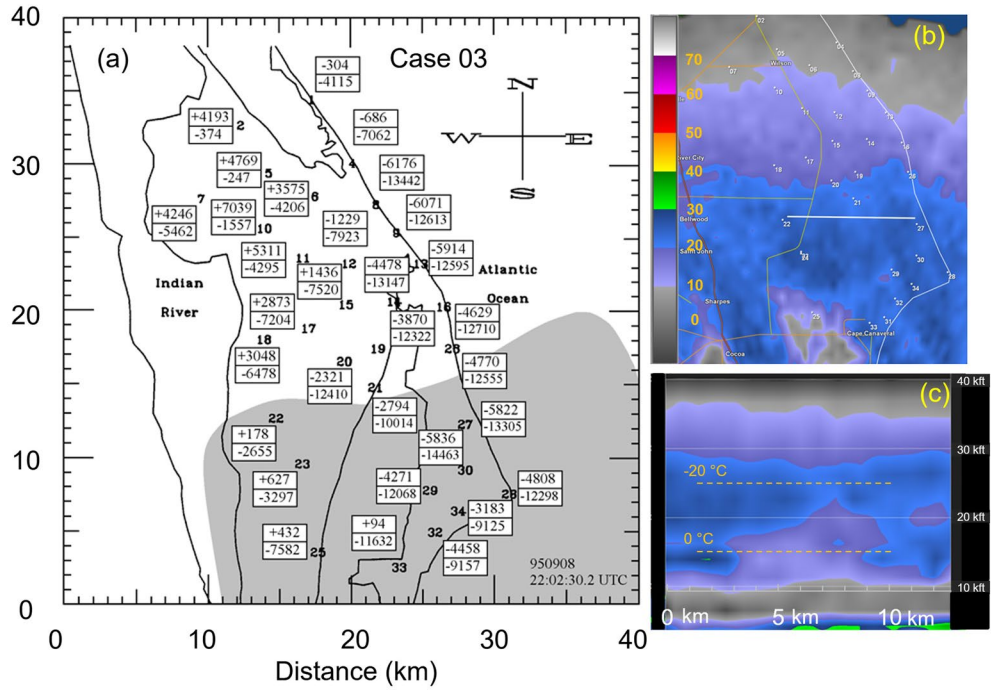

Figure 12. Radar reflectivity, flash envelope, and surface potential gradient for the long horizontal flash Case 3 on 8 September 1995, organized in as Figure 10.

the white line shown in the related PPI image. The cross-section regions were selected to explore the area where the flash ceased to propagate further into the KSC-ER domain. These cross-sections were also used in all cases to compute the MRR values included in Table 5. In all cases, MRR was at or above 20 dBZ, which is well-above the 7.5 dBZ threshold used in the LLCC.

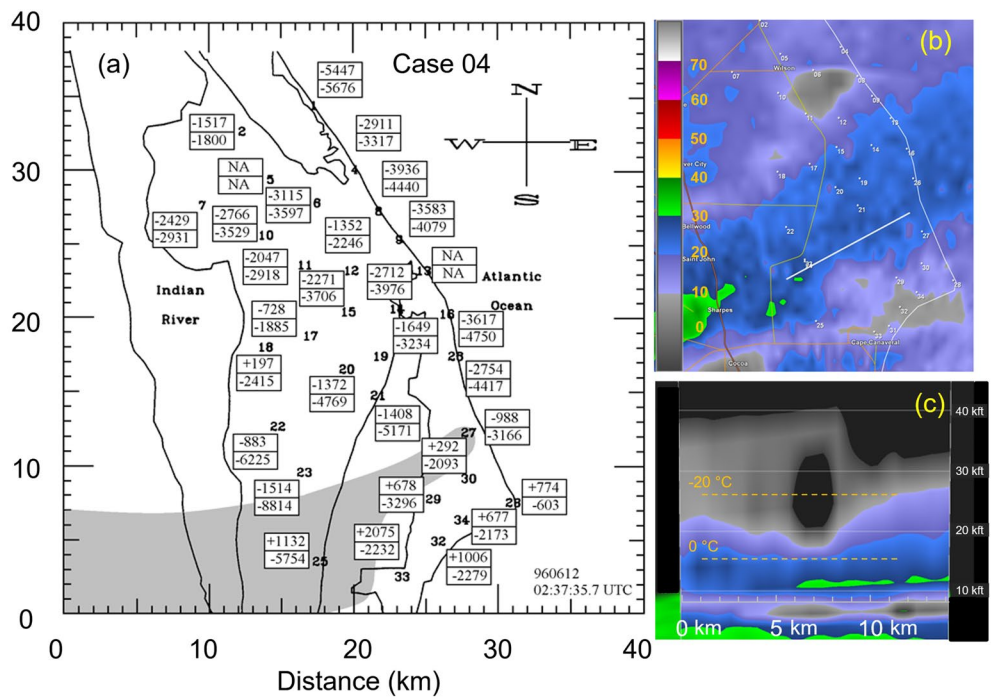

Figure 13. Radar reflectivity, flash envelope, and surface potential gradient for the long horizontal flash Case 4 on 12 June 1996, organized as in Figure 10.

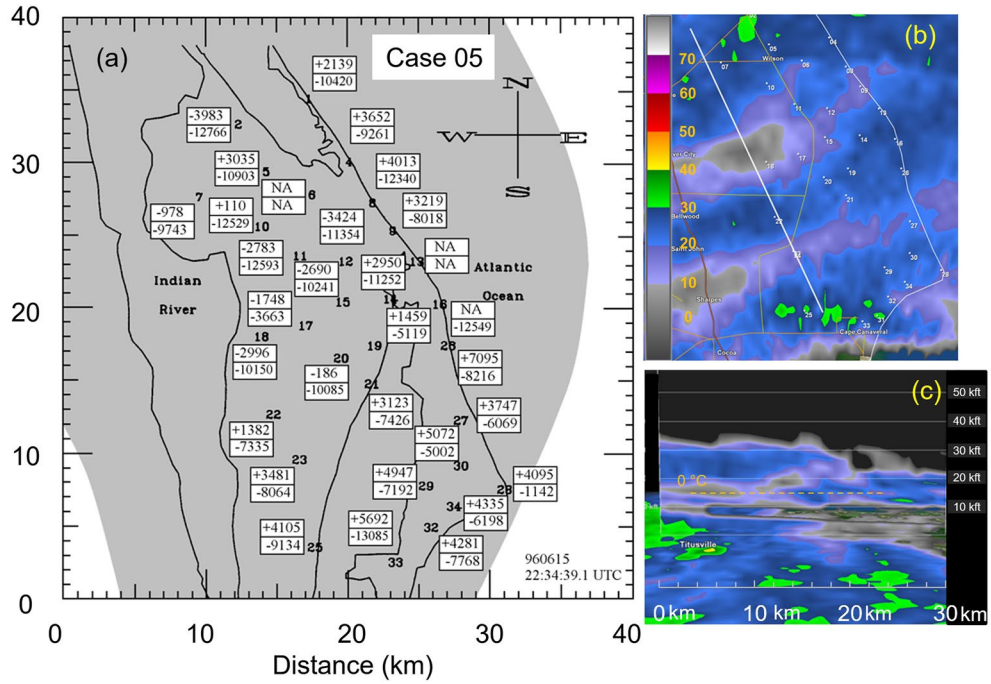

Figure 14. Radar reflectivity, flash envelope, and surface potential gradient for the long horizontal flash Case 5 on 15 June 1996, organized as in Figure 10.

It can be seen from Figures 10–18 that nearly all field mills exhibited high pre-flash readings, and that in most cases the values were well above 1,000 V/m. However, at least one field mill site within the network did not exceed the warning threshold in 11 out of 13 cases. Additionally, in 9 of the 13 cases, the majority of sites exhibited positive pre-flash PGs, but only two of these cases (Cases 2 and 6; Figures 11 and 15, respectively) exhibited

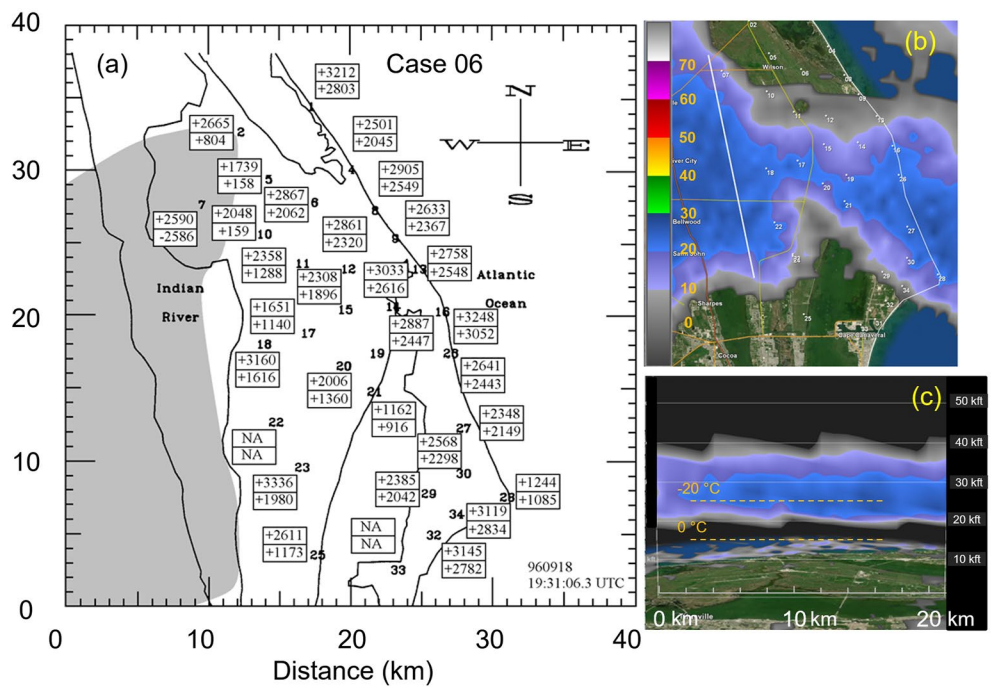

Figure 15. Radar reflectivity, flash envelope, and surface potential gradient for the long horizontal flash Case 6 on 18 September 1996, organized as in Figure 10.

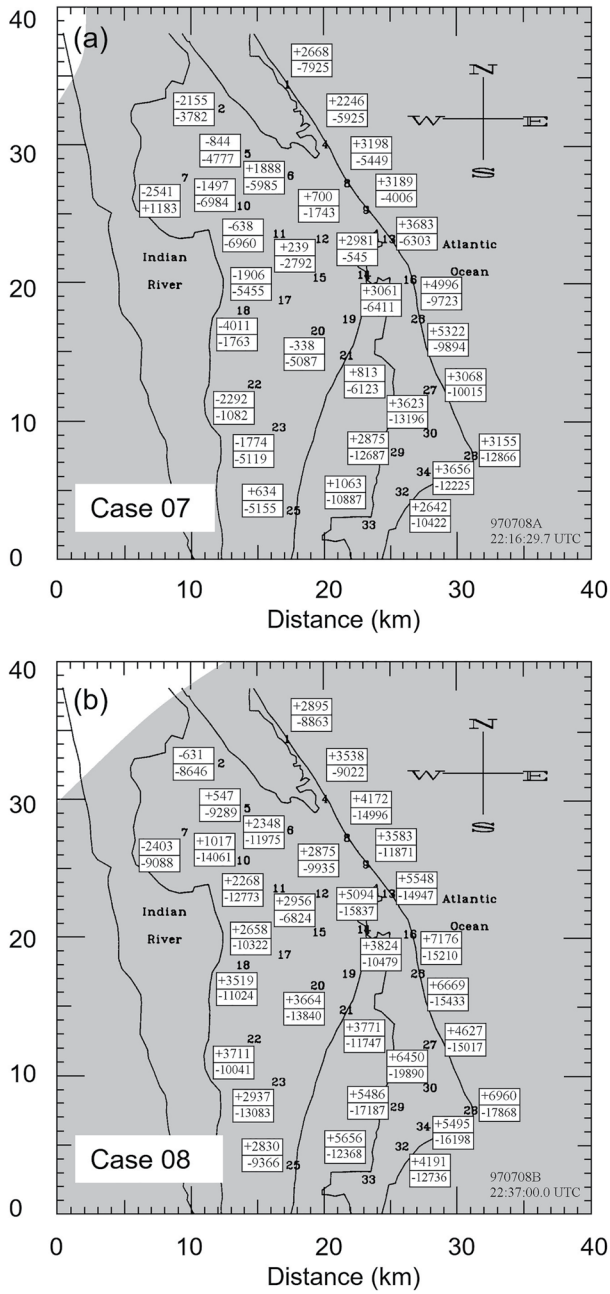

Figure 16. Surface potential gradient for two long horizontal flash Cases on 8 July 1997. Field values immediately prior to (upper value) and subsequent to (lower value) the flash are adjacent to the corresponding site ID. The shaded area represents the approximate aerial coverage (extent) of the flash.

positive pre-flash PGs at all sites. These same two flashes were the only cases where the magnitude of the pre-flash PG exceeded 1,000 V/m at all sites. In the remaining cases, the sites with low PG values (magnitude < 1,000 V/m) tended to be located between regions of high PGs of opposite polarity. An example of this behavior can be seen in Figure 16a (Case 7). This case exhibited high, positive pre-flash PGs in the eastern portion of the network and high, negative pre-flash PGs in the western portion of the network. Between these regions of opposite polarity, the pre-flash PGs were low (see sites 5, 11, 12, 15, 20, and 21).

The majority of flashes produced abrupt negative changes in PG, so the values after the flash were either negative, or more negative (i.e., less positive) than before the flash. The magnitude of the change ranged from a low of about 1 kV/m to a high of 25 kV/m. In 10 of the 13 cases, all sites showed a negative change in potential gradient following the flash. This observation suggests that positive charge was removed (or negative charge deposited) by most horizontal discharges. Interestingly, the flashes for Cases 7, 9, and 10 (Figures 16a, 17a, and 17b, respectively) produced a positive change in PG at one or more sites, with the flash for Case 9 (Figure 16a) resulting in a positive PG change at a majority of sites in the western part of the field mill network. Clearly, anvil and stratiform cloud charge structures can be complex, as noted by several researchers (Dye & Bansemer, 2019; Shepherd et al., 1996; Stolzenburg & Marshall, 2008).

10. Discussion and Conclusions

In this work we have evaluated the safety of the existing NASA launch constraints associated with surface potential gradient and precipitation radar measurements for two thunderstorm conditions: initial electrification in 13 cases of isolated air mass storms, and end-of-storm surface PG patterns before and after 13 long, horizontal lightning flashes in large decaying storms. During the initial electrification study, we found a surprisingly large percentage of cases that exhibited initial fair-weather field disturbances that caused us to explore these cases beyond the basic question of launch safety. A summary of findings and related conclusions for these conditions are provided in separate sub-sections below.

10.1. Isolated, Air Mass Thunderstorms

Initial disturbances in the surface PG produced by summer thunderstorms at the KSC-ER were seen 3.7–14.6 min prior to the first lightning discharge. In 11 of 13 cases, these disturbances initially had enhanced fair-weather polarity at one or more sites within 3.4 km of the storm center (first flash initiation) but were frequently negative at greater distances and at later times before the first flash. These results are consistent with the early formation of a localized, lower positive charge center (LPCC) in the cloud accompanied and followed by the development of a more-extensive negative charge region at higher altitudes. For the two cases with initial negative disturbances, the lead-time for lightning was near the minimum (1–2 min). This could be due to "masking" of the initial electrification because of a canceling of the surface foul-weather field by lower positive charge.

These findings are consistent with both mechanisms of initial positive charging discussed in Section 2.1 (graupel below the "reversal temperature" (Williams, 1989), and the liquid precipitation "drop breakup theory" promoted by Simpson and co-workers (Simpson & Robinson, 1941)), with the possibility that both (or even other) mechanisms contribute to varying degrees. We are inclined to prefer the reversal temperature mechanism, consistent with Williams (1989), Stolzenburg et al. (2015), and Saunders (2008). However, the complication here is that it

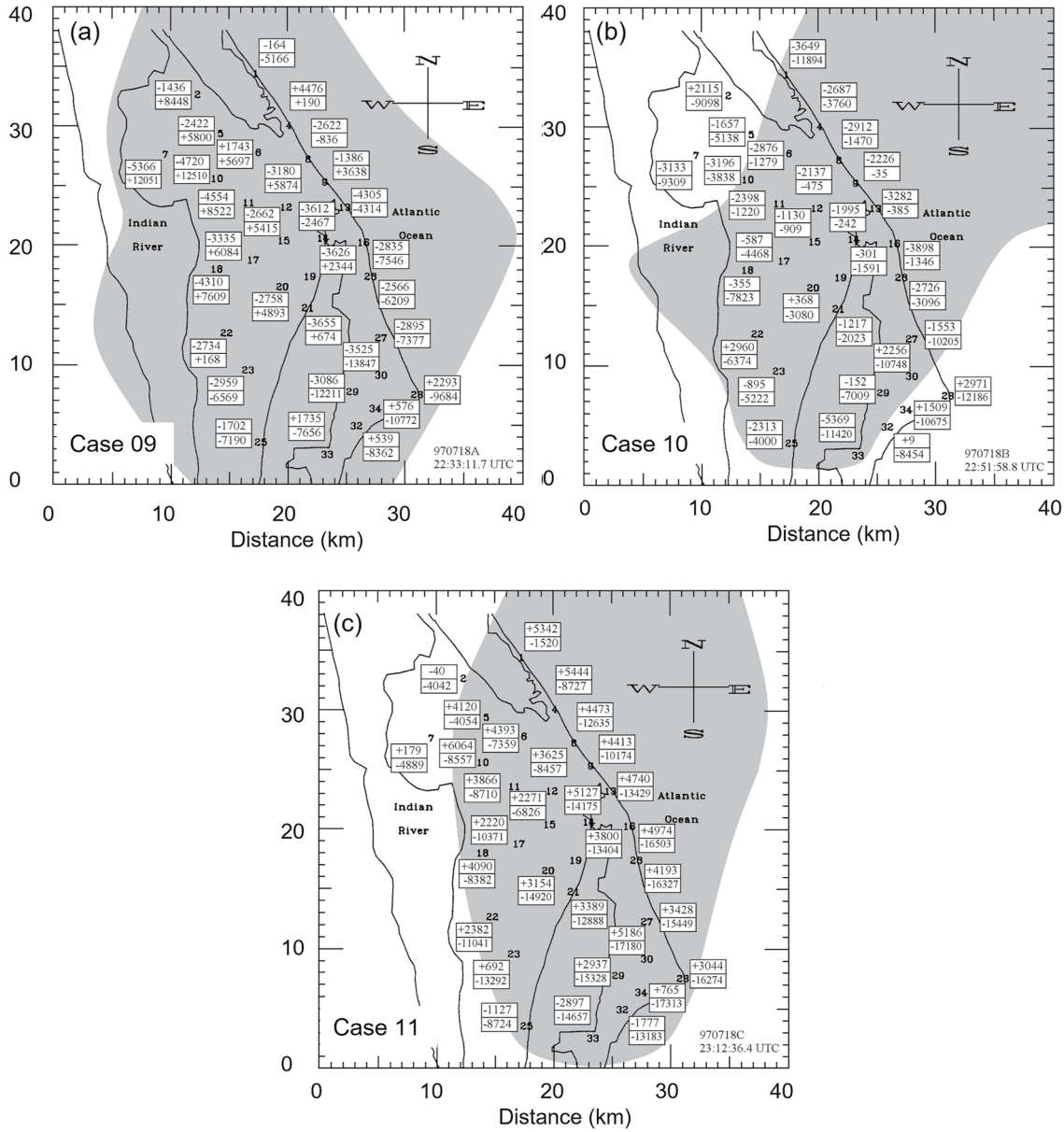

Figure 17. Surface potential gradient for three long horizontal flash Cases on 18 July 1997. Field values immediately prior to (upper value) and subsequent to (lower value) the flash are adjacent to the corresponding site ID. The shaded area represents the approximate aerial coverage (extent) of the flash.

might be difficult to produce sufficient graupel and ice crystals required for the charge reversal mechanism during the short time period (6–15 min) between the cloud top reaching −10°C and evidence of initial electrification in the surface PG measurement reported here (see Figure 9b). It is worth noting that aircraft observations of ice in developing Florida cumuli (Hallett et al., 1978) found that where updraft speeds were moderate (~6 ms^{-1}), the appearance of the ice phase (including graupel) occurred in the −4 to −6°C temperature height range within 5 min following cloud tops reaching −12°C (or warmer). The rapid growth rate of graupel was thought to be due to high concentrations of supercooled water droplets larger than 0.1 mm.

The largest initial + PG disturbances were seen by EFMs within 4 km of the storm center, but not always by the closest EFM. This suggests that the LPC regions are spatially small and may not be symmetrically distributed with respect to the storm center.

In 12 of the 13 cases, the first lightning discharge was an IC flash, and this in turn preceded the first CG by 1–24 min (typically 1–6 min). The onset of CG flashes frequently appeared after an increase in the positive

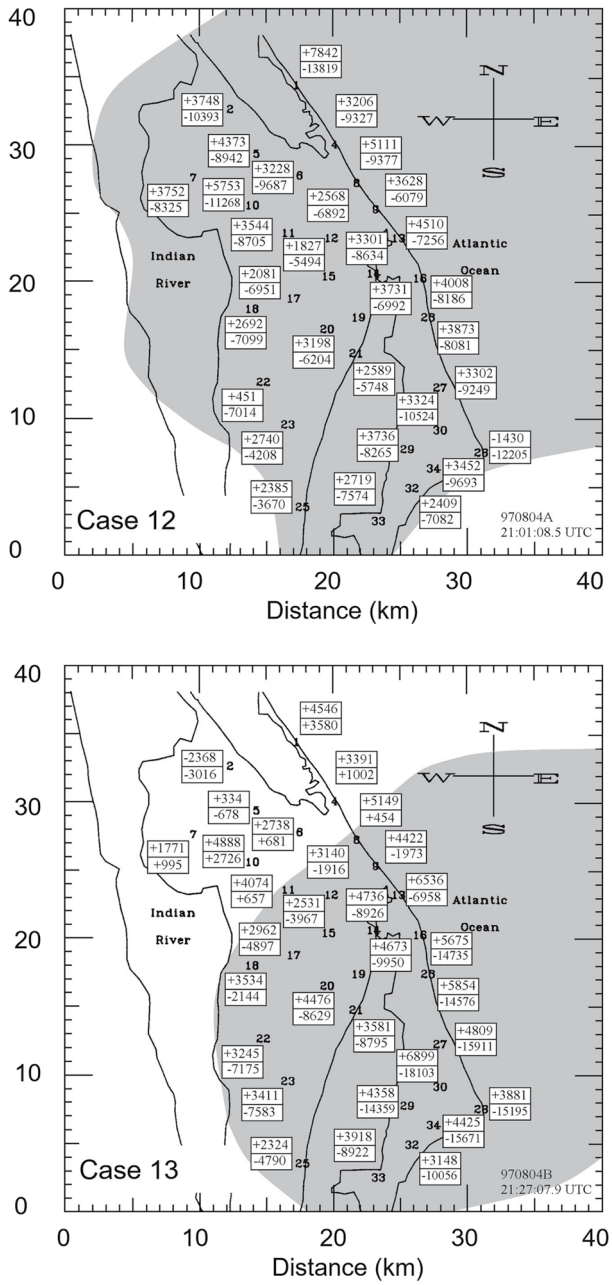

Figure 18. Surface potential gradient for two long horizontal flash Cases on 4 August 1997. Field values immediately prior to (upper value) and subsequent to (lower value) the flash are adjacent to the corresponding site ID. The shaded area represents the approximate aerial coverage (extent) of the flash.

(fair-weather) potential gradient that was produced either slowly by the process of cloud electrification, or abruptly by one or more IC discharges.

In all 13 cases, the electric field (PG) thresholds specified in the LLCC were crossed in the 15 min before the first lightning flash, that is, exceeded −100 or +500 V/m before the discharge. In 7 of 13 cases, the +500 V/m threshold was crossed and in 8 of 13 cases the −100 V/m threshold was crossed. However, during four storms (Cases 1, 2, 5, and 13), just one or two field mill sites violated at least one the threshold criterion. Thus, the electric field hazard criteria in the LLCC was only marginally safe in 4 out of 13 cases. This finding does not have an impact on the overall safety of the "Cumulus Rule" stated in Section 7, since this rule is based on cloud top temperature. It does clearly demonstrate that for warning purposes, monitoring surface electric fields would not be sufficient by itself.

Table 4 shows a large variation in the in lag-time (2.2–26 min) of the first CG flash after there was a clearly elevated surface PG (Big-E). Review of the related storm conditions in Table 1 shows that the two cases with lag-times below 3.3 min (Cases 7 and 8) were for cells within 4.6 km of other cells during their initial development. Conversely, Case 3 had the longest lag-time (26.4 min) and had the greatest distance to other cells (34.5 km—see Table 1). This finding is consistent with work by MacGorman et al. (2007) showing that CG flash occurrence and rate were "enhanced" by the existence of other nearby cells.

Launch safety during cumulus development is assured in the LLCC by observations of cloud top temperature that can be derived visually or using radar reflectivity. Launch through a developing cumulus is prohibited if the cloud top is colder than −5°C. In this work, we found that there were no surface-field indications of electrification (or lightning) until at least 6 min after the 0 dBZ cloud top reached −10°C (see Figures 8 and 9). In two cases, there was evidence of initial electrification before the 0 dBZ cloud top reached −20°C, with lightning occurring at least 12 min after both conditions.

A common radar parameter used for lightning warning is the time when reflectivity at some above-freezing height exceeds some specified value. For this work, we employed a reflectivity:height metric of −10°C level exceeding 35 dBZ, consistent with Dye et al. (1989) and Salvador et al. (2020), among others. For 11 of the 13 KSC-ER cases studied here, this radar condition typically occurred near the time of the initial disturbance in PG, but before the PG reached a more-significant levels (Big-E)—see Figures 8 and 9d. The study by Mosier et al. (2011) found that lead-time before first lightning and probability-of-detection (POD) in the Houston TX area were at their maximum for a 30 dBZ reflectivity at the level of −10°C level (average of ~7 min and ~95%, respectively). However, this metric had false-alarm rates above 0.5. Increasing the threshold reflectivity to 35 dBZ reduced the false-alarm rate (FAR) but also reduced the average lead-time by one minute and the POD to below 85%. Our lead-time findings are generally consistent with these observations (8-min mean—see Figure 8), suggesting there is similar behavior in Texas and Florida. A later study by (Seroka et al. (2012) considered both IC and CG flashes in Florida, and found similar average lead times for CG lightning as Mosier et al. when using a (lower) threshold reflectivity of 20 dBZ at −10°C. CG flashes occurred 2.4 min later (on average) than IC flashes. Like the Mosier et al. study, they found competing requirements between FAR and POD for both flash types. The 10 dBZ threshold difference between these two studies may be due to a combination of local storm behavior (Texas vs. Florida coasts) and differences in the resolution of the constant-altitude PPI reflectivity (CAPPI) calculations used in these studies (1 km in Florida (Seroka) and 2 km in Texas (Mosier)). Interestingly, our findings relating reflectivity and lead-time are somewhat more

consistent with the Texas study. Both of these studies suggest that lower reflectivity (20–30 dBZ, vs. 36 dBZ) at the −10°C can result in cloud electrification and subsequent lightning, when compared to the findings by Dye et al. (1989) in New Mexico. This may be due to the use of CAPPIs rather than interpolated volume scans, or local meteorological differences (reduced low-level moisture and mountainous terrain for the New Mexico storms studied by Dye et al. (1989, 2007)). The Seroka et al. (2012) study in Florida suggests the possibility of lightning occurrence at much lower reflectivities than we saw in this study, and they have the benefit of having evaluated thousands of cases over a 4-year period.

10.2. Long, Horizontal Discharges

Surface PG and reflectivity measurements prior to 13 long, horizontal discharges that propagated into the KSC-ER domain showed that the LLCC constraints would have appropriately prevented launch through the impacted cloud volume. Surface PGs at most EFM sites exceeded the 1,000 V/m (magnitude) warning threshold. However, in 10 out of 13 cases, at least one field mill site within the flash perimeter did not exceed the warning threshold. Thus, single local field mills cannot provide sufficient warning about the risk of horizontal flashes overhead. Additionally, precipitation radar characterization of the reflectivity above the 0°C level correlated well with this risk, with above-freezing-level reflectivity values greater than 20 dBZ in regions reached by lightning channels. It is important to note that a small fraction of lightning flashes produced in anvils have been shown to extend up to 15 km beyond the 0 dBZ cloud edge (Fuelberg et al., 2014). It is not clear that surface PG will be elevated beneath these “clear air” lightning channels in such cases, so further study would be valuable.

The surface potential gradient immediately before 9 of 13 horizontally extensive flashes was predominately positive, and in 12 out of the 13 cases the change in potential gradient was negative at most sites. These results suggest that positive charge was removed (or negative charge was deposited) by most of the horizontally extensive flashes.

Data Availability Statement

Most of the source data from the LPLWS and LDAR systems were lost over the last two decades, so the only available data records are PDF electric field waveforms and limited LDAR flash plots in Microsoft Word. These data are placed in the University of Arizona online repository (Cummins, 2022). The spreadsheets, supporting data tables, and related MATLAB code are also provided in the repository. The specific level-II NEXRAD radar data (https://ncdc.noaa.gov/nexradinv) used in this study are also placed in this repository and are also available through the NOAA public S3 bucket on Amazon (https://noaa-nexrad-level2.s3.amazonaws.com). The radar data was analyzed using GR2Analyst (https://en.wikipedia.org/wiki/GRLevelX; https://grlevelxusers.com/faq/). Soundings were obtained from (http://weather.uwyo.edu/upperair/sounding.html).

Acknowledgments
The lightning and surface potential gradient analyses presented in this work was done by the first author (SCH) as part of his Master's research at the University of Arizona, completed in 2000. The second and third authors gratefully acknowledge partial support for this work by NASA Kennedy Space Center. The detailed and thoughtful review of the initial manuscript by Earle Williams led to a much clearer and coherent treatment of the work in the final manuscript. We also thank Dr. Williams for discussions related to drop breakup as a candidate for creating the early fair-weather field deflections. Discussions with Dr. Greg Seroka helped us understand the trade-off between POD and FAR in his 2012 lightning nowcasting study.

References

Arabian, D. D. (1970). Aspects of the Apollo 12 lightning incident. *SAE Technical Papers*, *79*, 2852–2859. https://doi.org/10.4271/700938

Atlas, D. (1958). Radar lightning echoes and atmospherics in vertical cross section. In L. G. Smith (Ed.), *Recent advances in atmospheric electricity* (pp. 441–459). Pergamon Press.

Black, R. A., & Hallett, J. (1998). The mystery of cloud electrification. *American Scientist*, *86*(6), 526–534. https://doi.org/10.1511/1998.6.526

Boccippio, D. J., Heckman, S., & Goodman, S. J. (2001a). A diagnostic analysis of the Kennedy Space Center LDAR network 1. Data characteristics. *Journal of Geophysical Research Atmospheres*, *106*(D5), 4769–4786. https://doi.org/10.1029/2000JD900687

Boccippio, D. J., Heckman, S., & Goodman, S. J. (2001b). A diagnostic analysis of the Kennedy Space Center LDAR network 2. Cross-sensor studies. *Journal of Geophysical Research*, *106*(D5), 4787–4796. https://doi.org/10.1029/2000JD900688

Christian, H. J., Mazur, V., Fisher, B. D., Ruhnke, L. H., Crouch, K., & Perala, R. P. (1989). The Atlas/Centaur lightning strike incident. *Journal of Geophysical Research*, *94*(D11), 13169–13177. https://doi.org/10.1029/jd094id11p13169

Coleman, L. M., Marshall, T. C., Stolzenburg, M., Hamlin, T., Krehbiel, P. R., Rison, W., & Thomas, R. J. (2003). Effects of charge and electrostatic potential on lightning propagation. *Journal of Geophysical Research*, *108*(9), 1–27. https://doi.org/10.1029/2002jd002718

Coleman, L. M., Stolzenburg, M., Marshall, T. C., & Stanley, M. (2008). Horizontal lightning propagation, preliminary breakdown, and electric potential in New Mexico thunderstorms. *Journal of Geophysical Research*, *113*(9), 1–12. https://doi.org/10.1029/2007JD009459

Cummins, K. L. (2022). Data & Code for Manuscript "Surface Potential Gradients and NEXRAD Radar Reflectivities Before the Onset of Lightning at the KSC-ER" [Dataset]. University of Arizona Research Data Repository. https://doi.org/10.25422/azu.data.20349084.v1

Cummins, K. L., & Murphy, M. J. (2009). An overview of lightning locating systems: History, techniques, and data uses, with an in-depth look at the U.S. NLDN. *IEEE Transactions on Electromagnetic Compatibility*, *51*(3), 499–518. https://doi.org/10.1109/TEMC.2009.2023450

Dye, J. E., & Bansemer, A. (2019). Electrification in mesoscale updrafts of deep stratiform and anvil clouds in Florida. *Journal of Geophysical Research: Atmospheres*, *124*(2), 1021–1049. https://doi.org/10.1029/2018JD029130

Dye, J. E., Bateman, M. G., Christian, H. J., Defer, E., Grainger, C. A., Hall, W. D., et al. (2007). Electric fields, cloud microphysics, and reflectivity in anvils of Florida thunderstorms. *Journal of Geophysical Research*, *112*(11), 1–18. https://doi.org/10.1029/2006JD007550

Dye, J. E., Winn, W. P., Jones, J. J., & Breed, D. W. (1989). The electrification of New Mexico thunderstorms. 1. Relationship between precipitation development and the onset of electrification. *Journal of Geophysical Research*, *94*(D6), 8643–8656. https://doi.org/10.1029/JD094iD06p08643

Forbes, S. G., & Hoffert, S. G. (1999). Studies of Florida thunderstorms using LDAR, LLP, and single Doppler radar data. In H. J. Christian (Ed.), *Proceedings of the 11th international conference on atmospheric electricity* (pp. 496–499). NASA.

Fuelberg, H. E., Walsh, R. J., & Preston, A. D. (2014). The extension of lightning flashes from thunderstorms near Cape Canaveral, Florida. *Journal of Geophysical Research: Atmospheres*, *119*(16), 9965–9979. https://doi.org/10.1002/2014JD022105

Godfrey, R., Mathews, E. R., & McDivitt, J. A. (1970). *Analysis of Apollo 12 lightning incident*. NASA Technical Report. Marshall Space Flight Center. (TM-X-62894).

Hallett, J., Sax, R. I., Lamb, D., & Murty, A. S. R. (1978). Aircraft measurements of ice in Florida cumuli. *Quarterly Journal of the Royal Meteorological Society*, *104*(441), 631–651. https://doi.org/10.1002/qj.49710444108

Harrison, R. G. (2013). The carnegie curve. *Surveys in Geophysics*, *34*(2), 209–232. https://doi.org/10.1007/s10712-012-9210-2

Holden, D. N., Holmes, C. R., Moore, C. B., Winn, W. P., Cobb, J. W., Griswold, J. E., & Lytle, D. M. (1983). Local charge concentrations in thunderclouds. In L. H. Ruhnke & J. Latham (Eds.), *Proceedings in atmospheric electricity* (pp. 179–183). A. DeepackPublishing.

Jacobson, E. A., & Krider, E. P. (1976). Electrostatic field changes produced by Florida lightning. *Journal of the Atmospheric Sciences*, *33*(1), 103–117. https://doi.org/10.1175/1520-0469(1976)033<0103:EFCPBF>2.0.CO;2

Karunarathna, N., Marshall, T. C., Karunarathne, S., & Stolzenburg, M. (2017). Initiation locations of lightning flashes relative to radar reflectivity in four small Florida thunderstorms. *Journal of Geophysical Research: Atmospheres*, *122*(12), 6565–6591. https://doi.org/10.1002/2017JD026566

Klazura, G. E., & Imy, D. A. (1993). A description of the initial set of analysis products available from the NEXRAD WSR-88D system. *Bulletin of the American Meteorological Society*, *74*(7), 1293–1311. https://doi.org/10.1175/1520-0477(1993)074<1293:ADOTIS>2.0.CO;2

Koshak, J., & Krider, E. P. (1989). Analysis of lightning field changes during active Florida thunderstorms. *Journal of Geophysical Research*, *94*(D1), 1165–1186. https://doi.org/10.1029/jd094id01p01165

Krehbiel, P. R. (1986). The electrical structure of thunderstorms. In *The Earth's electrical environment* (pp. 90–113). National Academic Press.

Krider, E. P., Noggle, R. C., Pifer, A. E., & Vance, D. L. (1980). Lightning direction-finding systems for forest fire detection. *Bulletin of the American Meteorological Society*, *16*(9), 980–986. https://doi.org/10.1175/1520-0477(1980)061<0980:ldfsff>2.0.co;2

Kuhlman, K. M., MacGorman, D. R., Biggerstaff, M. I., & Krehbiel, P. R. (2009). Lightning initiation in the anvils of two supercell storms. *Geophysical Research Letters*, *36*(7), 1–5. https://doi.org/10.1029/2008GL036650

Lennon, C., & Maier, L. M. (1991). Lightning mapping system. In *1991 international aerospace and ground conference on lightning and static electricity* (pp. 89-1–89-10). NASA.

Lhermitte, R., & Krehbiel, P. R. (1979). Doppler radar and radio observations of thunderstorms. *IEEE Transactions on Geoscience Electronics*, *17*(4), 162–171. https://doi.org/10.1109/TGE.1979.294644

Ligda, M. G. H. (1956). The radar observation of lightning. *Journal of Atmospheric and Terrestrial Physics*, *9*(5–6), 329–330. https://doi.org/10.1016/0021-9169(56)90152-0

Livingston, J. M., & Krider, E. P. (1978). Electric fields produced by Florida thunderstorms. *Journal of Geophysical Research*, *83*(C1), 385. https://doi.org/10.1029/jc083ic01p00385

Lucas, G. M., Thayer, J. P., & Deierling, W. (2017). Statistical analysis of spatial and temporal variations in atmospheric electric fields from a regional array of field mills. *Journal of Geophysical Research: Atmospheres*, *122*(2), 1158–1174. https://doi.org/10.1002/2016JD025944

MacGorman, D. R., Apostolakopoulos, I. R., Lund, N. R., Demetriades, N. W. S., Murphy, M. J., & Krehbiel, P. R. (2011). The timing of cloud-to-ground lightning relative to total lightning activity. *Monthly Weather Review*, *139*(12), 3871–3886. https://doi.org/10.1175/MWR-D-11-00047.1

MacGorman, D. R., Filiaggi, T., Holle, R. L., & Brown, R. A. (2007). Negative cloud-to-ground lightning flash rates relative to VIL, maximum reflectivity, cell height, and cell isolation. *Journal of Lightning Research*, *1*(January), 132–147.

MacGorman, D. R., & Rust, W. D. (1998). *The electrical nature of storms*. Oxford University Press.

MacGorman, D. R., Taylor, W. L., & Few, A. (1983). Lightning location from acoustic and VHF techniques relative to storm structure from 10-cm radar. In L. H. Ruhnke & J. Latham (Eds.), *Proceedings in atmospheric electricity* (pp. 377–380). A. Deepack Publishing.

Maier, L. M., & Krider, E. P. (1986). The charges that are deposited by cloud-to-ground lightning in Florida. *Journal of Geophysical Research*, *91*(D12), 13275. https://doi.org/10.1029/jd091id12p13275

Maier, L. M., Lennon, C., Britt, T., & Schaefer, S. (1995). Lightning detection and ranging (LDAR) system performance analysis. In *6th conference on aviation weather systems*. American Meteorological Society.

Maier, L. M., Lennon, C., Krehbiel, P., Stanley, M., & Robison, M. (1995). Comparison of lightning and radar observations from the KSC LDAR and NEXRAD radar. In *17th conference on radar meteorology* (pp. 648–650). American Meteorological Society.

Marshall, T. C., Stolzenburg, M., Krehbiel, P. R., Lund, N. R., & Maggio, C. R. (2009). Electrical evolution during the decay stage of New Mexico thunderstorms. *Journal of Geophysical Research*, *114*(2), 1–20. https://doi.org/10.1029/2008JD010637

Mattos, E. V., Machado, L. A. T., Williams, E. R., Goodman, S. J., Blakeslee, R. J., & Bailey, J. C. (2017). Electrification life cycle of incipient thunderstorms. *Journal of Geophysical Research: Atmospheres*, *122*(8), 4670–4697. https://doi.org/10.1002/2016JD025772

Mazur, V., & Rust, W. D. (1983). Lightning propagation and flash density in squall lines as determined with radar. *Journal of Geophysical Research*, *88*(C2), 1495–1502. https://doi.org/10.1029/JC088iC02p01495

Mecikalski, R. M., & Carey, L. D. (2018). Radar reflectivity and altitude distributions of lightning as a function of IC, CG, and HY flashes: Implications for LNOx production. *Journal of Geophysical Research: Atmospheres*, *123*(22), 12814–12828. https://doi.org/10.1029/2018JD029238

Medina, B. L., Carey, L. D., Lang, T. J., Bitzer, P. M., Deierling, W., & Zhu, Y. (2021). Characterizing charge structure in Central Argentina thunderstorms during RELAMPAGO utilizing a New charge layer polarity identification method. *Earth and Space Science*, *8*(8), e2021EA001803. https://doi.org/10.1029/2021EA001803

Merceret, F. J., Willett, J. C., Christian, H. J., Dye, J. E., Krider, E. P., Madura, J. T., et al. (2010). A history of the lightning launch commit criteria and the lightning advisory panel for America's space program. Retrieved from https://ntrs.nasa.gov/citations/20110000675

Mo, Q., Helsdon, J. H., & Winn, W. P. (2002). Aircraft observations of the creation of lower positive charges in thunderstorms. *Journal of Geophysical Research*, *107*(22), 4616. ACL 4-1-ACL 4-15. https://doi.org/10.1029/2002JD002099

Moore, C. B., & Vonnegut, B. (1977). The thundercloud. In *Lightning: Physics of lightning* (Vol. 1, p. 64-9). Academic Press.

Mosier, R. M., Schumacher, C., Orville, R. E., & Carey, L. D. (2011). Radar nowcasting of cloud-to-ground lightning over Houston, Texas. *Weather and Forecasting*, *26*(2), 199–212. https://doi.org/10.1175/2010WAF2222431.1

Murphy, M. J. (1996). *The electrification of Florida thunderstorms* (Ph.D. dissertation). University of Arizona.
Murphy, M. J., Krider, E. P., & Maier, M. W. (1996). Lightning charge analyses in small Convection and Precipitation Electrification (CaPE) experiment storms. *Journal of Geophysical Research*, *101*(23), 29615–29626. https://doi.org/10.1029/96jd01538
NASA-STD-4010. (2017). NASA standard for lightning launch Commit criteria for space flight. Retrieved from https://standards.nasa.gov/standard/nasa/nasa-std-4010
Ogawa, T., & Brook, M. (1969). Charge distribution in thunderstorm clouds. *Quarterly Journal of the Royal Meteorological Society*, *95*(405), 513–525. https://doi.org/10.1002/qj.49709540505
Pawar, S. D., & Kamra, A. K. (2007). End-of-storm oscillation in tropical air mass thunderstorms. *Journal of Geophysical Research*, *112*(3), 1–8. https://doi.org/10.1029/2005JD006997
Peterson, M. (2021). Where are the most extraordinary lightning megaflashes in the Americas? *Bulletin of the American Meteorological Society*, *102*(3), E660–E671. https://doi.org/10.1175/BAMS-D-20-0178.1
Phillips, V. T. J., Formenton, M., Kanawade, V. P., Karlsson, L. R., Patade, S., Sun, J., et al. (2020). Multiple environmental influences on the lightning of cold-based continental cumulonimbus clouds. Part I: Description and validation of model. *Journal of the Atmospheric Sciences*, *77*(12), 3999–4024. https://doi.org/10.1175/JAS-D-19-0200.1
Pierce, E. T. (1955). The development of lightning discharges. *Quarterly Journal of the Royal Meteorological Society*, *81*(348), 229–240. https://doi.org/10.1002/qj.49708134809
Proctor, D. E. (1971). Hyperbolic system for obtaining VHF radio pictures of lightning. *Journal of Geophysical Research*, *76*(6), 1478–1489. https://doi.org/10.1029/jc076i006p01478
Proctor, D. E. (1983). Lightning and precipitation in a small multicellular thunderstorm. *Journal of Geophysical Research*, *88*(C9), 5421–5440. https://doi.org/10.1029/JC088iC09p05421
Rakov, V. A., & Uman, M. A. (2003). *Lightning physics and effects*. Cambridge University Press.
Reynolds, S. E., & Brook, M. (1956). Correlation of the initial electric field and the radar echo in thunderstorms. *Journal of Meteorology*, *13*(4), 376–380. https://doi.org/10.1175/1520-0469(1956)013<0376:cotief>2.0.co;2
Rison, W., Thomas, R. J., Krehbiel, P. R., Hamlin, T., & Harlin, J. (1999). A GPS-based three-dimensional lightning mapping system: Initial observations in central New Mexico. *Geophysical Research Letters*, *26*(23), 3573–3576. https://doi.org/10.1029/1999GL010856
Salvador, A., Pineda, N., Montanyà, J., & Solà, G. (2020). Seasonal variations on the conditions required for the lightning production. *Atmospheric Research*, *243*, 104981. https://doi.org/10.1016/j.atmosres.2020.104981
Saunders, C. (2008). Charge separation mechanisms in clouds. *Space Science Reviews*, *137*(1–4), 335–353. https://doi.org/10.1007/s11214-008-9345-0
Scott, R., Krehbiel, P., Stanley, M., & McCrary, S. (1995). Relation of lightning channels to storm structure from interferometer and dual-polarization radar observations. In *International conference on radar meteorology* (pp. 645–647).
Seroka, G. N., Orville, R. E., & Schumacher, C. (2012). Radar nowcasting of total lightning over the Kennedy Space Center. *Weather and Forecasting*, *27*(1), 189–204. https://doi.org/10.1175/WAF-D-11-00035.1
Shao, X. M., & Krehbiel, P. R. (1996). The spatial and temporal development of intracloud lightning. *Journal of Geophysical Research*, *101*(21), 26641–26668. https://doi.org/10.1029/96jd01803
Shepherd, T. R., Rust, W. D., & Marshall, T. C. (1996). Electric fields and charges near 0°C in. *Stratiform Clouds*, *124*(May), 919–938. https://doi.org/10.1175/1520-0493(1996)124<0919:efacni>2.0.co;2
Simpson, G. C. (1909). On the electricity of rain and its origin in thunderstorms. *Philosophical Transactions of the Royal Society of London*, *209*(441–458), 379–413. https://doi.org/10.1098/rsta.1909.0015
Simpson, G. C. (1927). The mechanism of a thunderstorm. *Proceedings of the Royal Society of London*, *114*(8), 376–401. https://doi.org/10.1175/1520-0493(1928)56<311:tmoat>2.0.co;2
Simpson, G. C., & Robinson, G. D. (1941). The distribution of electricity in thunderclouds, II. *Proceedings of the Royal Society of London*, *177*, 281–329. https://doi.org/10.5636/jgg.1.22
Simpson, G. C., & Scrase, F. J. (1937). The distribution of electricity in thunderclouds. *Proceedings of the Royal Society of London*, *1161*, 309–352. https://doi.org/10.5636/jgg.1.22
Stolzenburg, M., & Marshall, T. C. (2008). Charge structure and dynamics in thunderstorms. *Space Science Reviews*, *137*(1–4), 355–372. https://doi.org/10.1007/s11214-008-9338-z
Stolzenburg, M., Marshall, T. C., & Krehbiel, P. R. (2010). Duration and extent of large electric fields in a thunderstorm anvil cloud after the last lightning. *Journal of Geophysical Research*, *115*(19), 1–16. https://doi.org/10.1029/2010JD014057
Stolzenburg, M., Marshall, T. C., & Krehbiel, P. R. (2015). Initial electrification to the first lightning flash in New Mexico thunderstorms. *Journal of Geophysical Research: Atmospheres*, *120*(21), 11253–11276. https://doi.org/10.1002/2015JD023988
Stolzenburg, M., Marshall, T. C., Rust, W. D., & Bartels, D. L. (2002). Two simultaneous charge structures in thunderstorm convection. *Journal of Geophysical Research Atmospheres*, *107*(18), ACL 5-1–ACL 5-12. https://doi.org/10.1029/2001JD000904
Stolzenburg, M., Rust, W. D., & Marshall, T. C. (1998). Electrical structure in thunderstorm convective regions 2. Isolated storms. *Journal of Geophysical Research*, *103*(D12), 14079–14096. https://doi.org/10.1029/97JD03547
Teer, T. L., & Few, A. A. (1974). Horizontal lightning. *Journal of Geophysical Research*, *79*(24), 3436–3441. https://doi.org/10.1029/jc079i024p03436
Thomas, R. J., Krehbiel, P. R., Rison, W., Hunyady, S. J., Winn, W. P., Hamlin, T., & Harlin, J. (2004). Accuracy of the lightning mapping array. *Journal of Geophysical Research*, *109*(14), D14207. https://doi.org/10.1029/2004JD004549
Van Der Velde, O. A., Montanyà, J., Soula, S., Pineda, N., & Bech, J. (2010). Spatial and temporal evolution of horizontally extensive lightning discharges associated with sprite-producing positive cloud-to-ground flashes in northeastern Spain. *Journal of Geophysical Research*, *115*(9), 1–17. https://doi.org/10.1029/2009JA014773
Vonnegut, B., Moore, C. B., & Botka, A. T. (1959). Preliminary results of an experiment to determine initial precedence of organized electrification and precipitation in thunderstorms. *Journal of Geophysical Research*, *64*(3), 347–357. https://doi.org/10.1029/jz064i003p00347
Wang, F., Liu, H., Dong, W., Zhang, Y., Yao, W., & Zheng, D. (2019). Radar reflectivity of lightning flashes in stratiform regions of mesoscale convective systems. *Journal of Geophysical Research: Atmospheres*, *124*(24), 14114–14132. https://doi.org/10.1029/2019JD031238
Wang, F., Zhang, Y., Liu, H., Dong, W., Yao, W., & Zheng, D. (2020). Vertical reflectivity structures near lightning flashes in the stratiform regions of mesoscale convective systems. *Atmospheric Research*, *242*(August 2019), 104961. https://doi.org/10.1016/j.atmosres.2020.104961
Weiss, S. A., MacGorman, D. R., & Calhoun, K. M. (2012). Lightning in the anvils of supercell thunderstorms. *Monthly Weather Review*, *140*(7), 2064–2079. https://doi.org/10.1175/mwr-d-11-00312.1
Willett, J. C., Merceret, F. J., Krider, E. P., O'Brien, T. P., Dye, J. E., Walterscheid, R. L., et al. (2016). Rationales for the lightning launch commit criteria. Retrieved from https://ntrs.nasa.gov/citations/20170001583

Williams, E. R. (1989). The tripole structure of thunderstorms. *Journal of Geophysical Research*, *94*(D11), 13151–13167. https://doi.org/10.1029/jd094id11p13151

Williams, E. R. (1998). The positive charge reservoir for sprite-producing lightning. *Journal of Atmospheric and Solar-Terrestrial Physics*, *60*(7–9), 689–692. https://doi.org/10.1016/S1364-6826(98)00030-3

Williams, E. R. (2009). CTR Wilson versus GC Simpson: Fifty years of controversy in atmospheric electricity. *Atmospheric Research*, *91*(2–4), 259–271. https://doi.org/10.1016/j.atmosres.2008.03.024

Williams, E. R., Weber, M. E., & Orville, R. E. (1989). The relationship between lightning type and convective state of thunderclouds. *Journal of Geophysical Research*, *94*(D11), 13213. https://doi.org/10.1029/jd094id11p13213

Wilson, C. T. R. (1920). Investigations on lightning discharges and on the electric field of thunderstorms. *Philosophical Transactions of the Royal Society of London*, *221*(582–593), 73–115.

Wilson, C. T. R. (1929). Some thundercloud problems. *Journal of the Franklin Institute*, *208*(1), 1–12. https://doi.org/10.1016/S0016-0032(29)90935-2

Wilson, J. G., Cummins, K. L., & Krider, E. P. (2009). Small negative cloud-to-ground lightning reports at the NASA Kennedy Space Center and air force eastern range. *Journal of Geophysical Research*, *114*(24), D24103. https://doi.org/10.1029/2009JD012429

Workman, E. J., Holzer, R. E., & Pelsor, G. T. (1942). *The electrical structure of thunderstorms* Tech report 864. National Advisory Committee for Aeronautics.

Workman, E. J., & Reynolds, S. E. (1949). Electrical activity as related to thunderstorm cell growth. *Bulletin of the American Meteorological Society*, *30*(4), 142–144. Retrieved from https://www.jstor.org/stable/26258148